Defense Nuclear Agency
Alexandria, VA 22310-3398

DNA-TR-90-170

Metal-Metal Microfilamentary Composites for High Strength Electrical Conductor Applications - Phase II

James D. Klein, et al.
EIC Laboratories, Inc.
111 Downey Street
Norwood, MA 02062

August 1991

Technical Report

CONTRACT No. DNA 001-87-C-0150

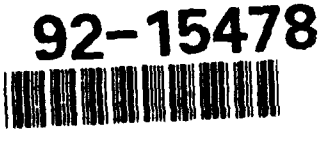

Destroy this report when it is no longer needed. Do not return to sender.

PLEASE NOTIFY THE DEFENSE NUCLEAR AGENCY, ATTN: CSTI, 6801 TELEGRAPH ROAD, ALEXANDRIA, VA 22310-3398, IF YOUR ADDRESS IS INCORRECT, IF YOU WISH IT DELETED FROM THE DISTRIBUTION LIST, OR IF THE ADDRESSEE IS NO LONGER EMPLOYED BY YOUR ORGANIZATION.

DISTRIBUTION LIST UPDATE

This mailer is provided to enable DNA to maintain current distribution lists for reports. We would appreciate your providing the requested information.

☐ Add the individual listed to your distribution list.

☐ Delete the cited organization/individual.

☐ Change of address.

NOTE:
Please return the mailing label from the document so that any additions, changes, corrections or deletions can be made more easily.

NAME: _____

ORGANIZATION: _____

OLD ADDRESS	CURRENT ADDRESS
_____	_____
_____	_____
_____	_____

TELEPHONE NUMBER: ( ) _____

SUBJECT AREA(s) OF INTEREST:

_____	_____
_____	_____
_____	_____

DNA OR OTHER GOVERNMENT CONTRACT NUMBER: _____

CERTIFICATION OF NEED-TO-KNOW BY GOVERNMENT SPONSOR (if other than DNA):

SPONSORING ORGANIZATION: _____

CONTRACTING OFFICER OR REPRESENTATIVE: _____

SIGNATURE: _____

CUT HERE AND RETURN

Director
Defense Nuclear Agency
ATTN: TITL
Washington, DC 20305-1000

Director
Defense Nuclear Agency
ATTN: TITL
Washington, DC 20305-1000

REPORT DOCUMENTATION PAGE

Form Approved OMB No. 0704-0188

1. AGENCY USE ONLY (Leave blank)	2. REPORT DATE	3. REPORT TYPE AND DATES COVERED
	910801	Technical 870908 - 900331

4. TITLE AND SUBTITLE

Metal-Metal Microfilamentary Composites for High Strength Electrical Conductor Applications - Phase II

5. FUNDING NUMBERS

C - DNA 001-87-C-0150
PE - 63221C
PR - SF
TA - SB
WV - DH035100

6. AUTHOR(S)

James D. Klein, Stuart F. Cogan, Allen Yen and Louis L. Wu

7. PERFORMING ORGANIZATION NAME(S) AND ADDRESS(ES)

EIC Laboratories, Inc.
111 Downey Street
Norwood, MA 02062

8. PERFORMING ORGANIZATION REPORT NUMBER

C915F

9. SPONSORING/MONITORING AGENCY NAME(S) AND ADDRESS(ES)

Defense Nuclear Agency
6801 Telegraph Road
Alexandria, VA 22310-3398
RAEV/Rodriguez

10. SPONSORING/MONITORING AGENCY REPORT NUMBER

DNA-TR-90-170

11. SUPPLEMENTARY NOTES

This work was sponsored by the Defense Nuclear Agency under RDT&E RMC Code B7661D SF SB 00034 RAEV 3230A 25904D.

12a. DISTRIBUTION/AVAILABILITY STATEMENT

Approved for public release; distribution is unlimited.

12b. DISTRIBUTION CODE

13. ABSTRACT *(Maximum 200 words)*

Continuous-filament Cu-Nb and Cu-Ag composites were fabricated as candidate high strength electrical conductors. Microfilamentary Cu-Nb composites achieved remarkable strength levels while maintaining good electrical conductivity. By examining the superconducting properties of the Cu-Nb composites, it was determined that some recovery processes were active in the Nb fibers at relatively low annealing temperatures. However, the fine-filament Cu-Nb wires exhibited excellent pulsed current capabilities. A novel testing regime called pulsed current fatigue demonstrated the impact of composite design and pulse conditions on pulsed current lifetime. Cu-Ag composites were fabricated to provide a higher conductivity alternative to Cu-Nb. Although the Cu-Ag results were promising, a second-generation composite is needed to extend the benefits to the highest strength levels.

14. SUBJECT TERMS

Metal-Matrix Composites
High Strength Wires
Microfilamentary Composites
Pulsed Current Fatigue

15. NUMBER OF PAGES

70

16. PRICE CODE

17. SECURITY CLASSIFICATION OF REPORT	18. SECURITY CLASSIFICATION OF THIS PAGE	19. SECURITY CLASSIFICATION OF ABSTRACT	20. LIMITATION OF ABSTRACT
UNCLASSIFIED	UNCLASSIFIED	UNCLASSIFIED	SAR

CLASSIFIED BY:

N/A since Unclassified

DECLASSIFY ON:

N/A since Unclassified

SUMMARY

The mechanical and electrical properties of continuous-filament Cu-Nb and Cu-Ag composites have been surveyed. The microfilamentary Cu-Nb composites were found to have excellent mechanical strength, good electrical conductivity, and substantial resistance to annealing. As such, the fine-filament Cu-Nb composites are excellent materials for high strength electrical conductors. By determining the superconducting properties of the Nb filaments, the annealing behavior of finely divided Nb was determined. To assess the suitability of the Cu-Nb composites for pulsed current applications, a novel testing method called pulsed current fatigue was implemented. The technique is unique in that it provides a cyclic thermo-mechanical loading with an extremely simple experimental apparatus.

Cu-Ag composites were fabricated to provide a higher conductivity alternative to the Cu-Nb system. The anticipated electrical conductivity advantage afforded by Ag filaments is confirmed. Indeed, extrapolation of their conductivity vs. strength behavior indicates that the advantage of Cu-Ag over Cu-Nb will increase at the higher strength levels. However, Ag is not as aggressive as Nb with regard to developing strength by cold work. Although the present data suggests that higher strength levels can be accessed, the strengths of the Cu-Ag wires fabricated do not approach those of the best Cu-Nb samples.

TABLE OF CONTENTS

LIST OF ILLUSTRATIONS

LIST OF ILLUSTRATIONS (Continued)

LIST OF TABLES

SECTION 1

INTRODUCTION

Composite materials are generally employed because they afford a combination of properties not available in homogeneous samples. This is certainly the case for high strength electrical conductors. The electrical properties of high conductivity metals such as Cu or Ag are severely compromised when conventional strengthening techniques such as solid solution alloying or age hardening are applied. To retain the high electrical conductivity inherent in semi-noble metals the fcc phase must remain unalloyed. The available strengthening mechanisms are therefore reduced to cold work or composite microstructure. Cold work (work hardening) causes appreciable strengthening at the expense of increased resistivity brought on by the attendant increase in dislocation defect density. Composite microstructures also imply a higher overall resistivity because of the volume needed to accommodate the strengthening phase. Neither mechanism can successfully attain the high strength levels desired. However, if the two techniques are combined in a single design their synergistic effects can yield the desired strengthening.

The composite materials of this study were selected to obtain the best compromise between strength and conductivity in conductor applications. The deformation inherent in cold work procedures requires that the reinforcing phase be metallic. Moreover, the cable or wire geometry of most conductors suggest that maximum benefit will be realized when the reinforcing phase is present in the form of continuous fibers aligned with the wire axis. Maximum strengthening is generally afforded when the matrix and fiber materials have dissimilar crystal structures. Therefore, the majority of this study was performed using Nb (body-centered cubic or bcc) fibers in a Cu (face-centered cubic or fcc) matrix. However, the conductivity is least compromised when both phases are semi-noble. A brief investigation of Cu-Ag composites was included to probe this inviting alternative.

SECTION 2

SPECIFIC Cu-Nb COMPOSITES

The continuous filament composites of this study were fabricated by the Levi process as applied to Cu-Nb composites by Cline, Strauss, Rose, and Wulff (1). In this method OFHC Cu tubes are first swaged and then drawn onto Nb rods. The resulting monofilament composite is hex-drawn and cut into segments so that a billet can be assembled by stacking numerous hexes inside a Cu pipe. After the billet is evacuated and welded shut, extrusion and drawing operations are employed to reduce the composite to final wire size. Finer filament sizes can be achieved if additional bundling, extrusion, and reduction cycles are performed.

The three composite designs of this investigation were selected to demonstrate the performance differences attributable to filament size and volume fraction. The "2.0K" composite is a single extrusion design possessing 1956 filaments of 3.1 μm nominal diameter at a 0.0254 cm diameter wire size. A cross-section of a 0.049 cm (0.019 inch) diameter coarse-filament 2.0K composite wire is shown in Figure 1a. The hexagonal Cu core, thick perimeter can, and high 0.30 Nb volume fraction result in some crowding of the filaments in the conservative 2.0K design. The "1.8M" composite is a double extrusion design utilizing 709 colonies of 2479 filaments each to give 1.76 million filaments of 0.11 μm nominal diameter at a 0.0267 cm wire diameter. A scanning electron micrograph of the cross section of a 0.073 cm (0.029 inch) fine-filament 1.8M composite wire is shown in Figure 1b. Although the colony structure of this composite is readily discerned, the filaments are too small to be resolved at this magnification. Special efforts, such as centerless grinding of the first extrusion and use of a thinner perimeter can, allowed a more uniform filament distribution to minimize crowding in spite of the high 0.30 Nb volume fraction. The 2.2M composite is conceptually similar to the 1.8M design but differs in both number of filaments and Nb volume fraction. Because the 2.2M composite has 3055 filaments in each colony, it has a total of 2.17×10^6 filaments.

All of the composites of this study are continuous filament designs. Each filament is continuous throughout the length of the wire, whether the length be 1 cm or several kilometers. A significant benefit of the continuous design is an extraordinary uniformity of properties both along each wire's length and between wires of identical specification. Each filament of a given design has received the same deformation and should have uniform properties. However, there are three distinct Cu regions in each composite that are expected to have different physical characteristics. Because the interfilament Cu is finely partitioned by the Nb fibers, it receives severe mechanical deformation during wire drawing to final size. This allows the strength of the interfilament Cu to approach that of the Nb fibers at the finest wire sizes. Since the Cu layers between the colonies of the 1.8M and 2.2M composites are less severely constrained they should exhibit lower mechanical strength and electrical

(a)

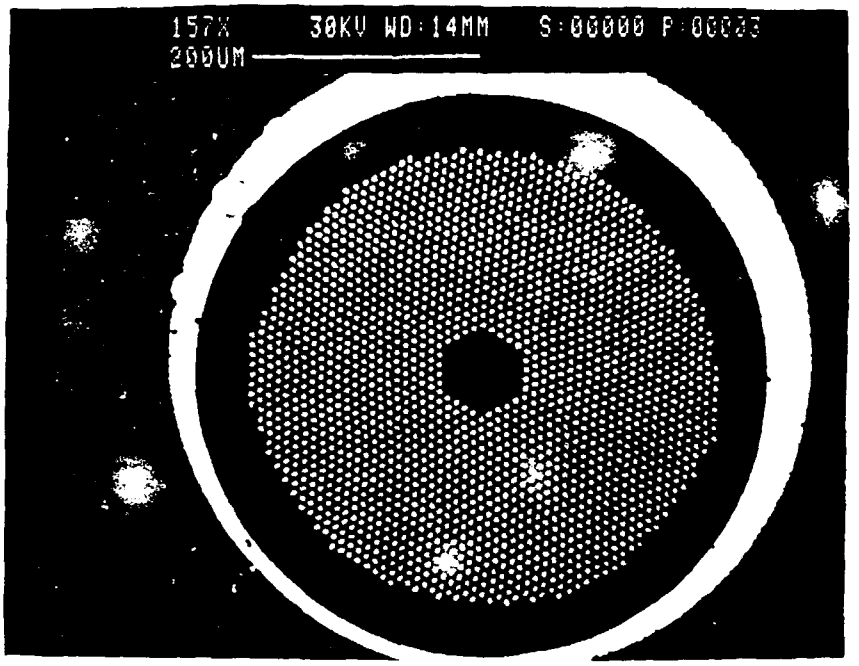

(b)

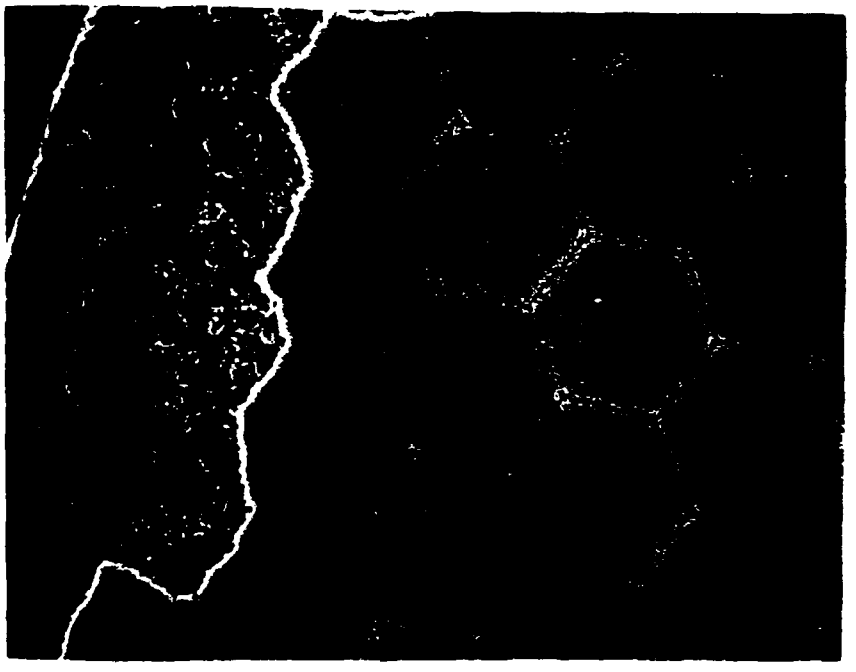

Figure 1. Cross-sections of (a) the 2.0K coarse-filament and (b) the 1.8M fine-filament Cu-Nb composites of this study. The 2.0K wire is derived from a single extrusion billet whereas the 1.8M material is the result of a double extrusion fabrication.

resistivity. The Cu in the filament-free perimeter can (and in the center of the 2.0K design) should exhibit strengthening and annealing characteristics approximating those of heavily deformed bulk OFHC Cu. As such, the perimeter Cu can is a region of relatively low mechanical strength and high electrical conductivity. This is useful because it both enhances ac electrical conductivity and minimizes notch sensitivity. Because of the differences in filament size, filament count, and Nb volume fraction the three Cu-Nb composites provide a basis for the assessment of design parameters. The specifications of the composites are summarized in Table 1.

Table 1. Design parameters for the 2.0K, 1.8M, and 2.2M Cu-Nb composite wires.

Composite Designation	2.0K	1.8M	2.2M
Number of Colonies	1	709	709
Filaments per Colony	1956	2479	3055
Total Number of Filaments	1956	1.76×10^6	2.17×10^6
Overall Nb Volume Fraction	0.30	0.30	0.18
Local Nb Volume Fraction	0.45	0.35	0.23
Nominal Fiber Diameter at 0.0254 cm wire size	3.1 μm	0.11 μm	0.07 μm

SECTION 3

STRENGTH AND RESISTIVITY OF Cu-Nb COMPOSITES

3.1 CONCEPT AND APPROACH.

The two most important parameters for a robust electrical conductor are mechanical strength and electrical resistivity. In particular a high mechanical strength and low electrical resistivity are desired. Additionally, any normal-state conductor experiences resistance or Joule heating while carrying a current. In many environments the available cooling may be insufficient to maintain the ambient temperature in the conductor. Therefore, the annealing behavior of the conductors can be important.

Filamentary composites of continuous Nb fibers in Cu matrices were tested to determine the effect of composite design on ultimate tensile strength and electrical resistivity. Both coarse and fine filament composites were tested to demonstrate the benefits of microfilamentary composites. Properties were determined as a function of wire size to indicate the strengthening mechanisms. Fine-filament wires of various diameters given elevated-temperature heat treatments were tensile tested to define annealing characteristics.

3.2 INTRODUCTION.

The strength and annealing characteristics of multifilamentary composites have been investigated in a number of Cu-matrix systems such as Cu-W (2), Cu-Ag (3,4), and Cu-Nb (5,6). However, most studies of fine-filament composites have been performed on materials fabricated by *in-situ* methods (3-7) to facilitate the preparation of fine-filament sizes. The strengths of large filament designs tend to obey the rule of mixtures (2), whereas the tensile values of fine-filament composites often exceed linear combination predictions by large margins in both fcc-fcc (3) and fcc-bcc (5) systems. Additionally, the electrical resistivity has exhibited anomalous effects at the high reductions required to obtain fine fiber sizes (4).

The mechanisms by which the physical properties are enhanced can be revealed by examining the functionality of strength and resistivity increases with respect to decreasing wire size. The simultaneous deformation of bcc Nb and fcc Cu necessarily requires some accommodation between matrix and filaments. Specifically, the [110] texture which develops in bcc metals (8) results in a marked tendency of the Nb filaments to become ribbon shaped in *in-situ* Cu-Nb composites (5). Since the partitioning and high dislocation density in the matrix result in high Cu resistivities, electrical conductivity is a useful means of observing matrix annealing in these materials. The elevated-temperature results of Karasek and Bevk (6) indicate that even very fine *in-situ* Cu-Nb wires are annealed by 525°C. Further work on these materials by Bevk, Harbison, and Bell (5) demonstrated ultimate tensile strengths that far exceed

the rule of mixtures. Continuous-filament resistivity results of Klein and Rose (9) indicate that the finest composites are not completely annealed until 600°C. By monitoring ultimate tensile strength and electrical resistivity as a function of Nb volume fraction and wire size the available tradeoffs between mechanical and electrical properties are to be defined. Examination of annealing behavior will indicate suitability for elevated temperature service.

3.3 RESULTS AND DISCUSSION.

Tensile testing of continuous filament Cu-Nb composites was undertaken to define the manner in which strength was developed. Of particular interest were the effects of filament size and Nb volume fraction. Wire samples of the three composite designs were tensile tested in an Instron 4204 loadframe until failure. The 2.0K and 1.8M wires provide a comparison of coarse and fine filament composites of similar Nb volume fraction. Including both 1.8M and 2.2M wires provided a basis for assessing the role of Nb volume fraction in determining strength. Wire drawing is a permanent deformation process that reduces the dimensions of the wire cross-section uniformly. As the diameter of the wire decreases the distance between the Cu matrix-Nb filament interfaces is reduced. Such reductions in the scale d of the microstructure usually increase the strength σ of a material according to the Hall-Petch relationship (10,11)

$$\sigma = \sigma_o + \frac{k}{\sqrt{d}}$$

where σ_o and k are constants for a given material. To reveal any tendency of the data to follow this trend the ultimate tensile strength was plotted as a function of root reciprocal wire diameter. The ultimate tensile strengths of the sample wires are noted in Figure 2. The 2.0K strengths are linear with respect to root reciprocal wire size throughout the diameter range investigated. Thus, the coarse-filament 2.0K data can be described well by a Hall-Petch relationship. The fine-filament 1.8M and 2.2M curves exhibit a significantly different behavior. As anticipated, the fine-filament wires are remarkably stronger than the 2.0K wires. In addition, the rate of increase in strength (the slope) is much greater for the fine-filament data. The higher Nb volume fraction 1.8M wires are stronger than their 2.2M counterparts at similar wire sizes. However, the fine-filament curves are linear only over the first part of the size range. Curves for both 1.8M and 2.2M wires become parabolic at the finest wire sizes. It becomes obvious that other factors are playing a role in strengthening the composites.

The deformation inherent in room temperature wire drawing introduces a large degree of cold work in the composite wires. The major influence of this deformation on the microstructure is to increase dramatically the density of

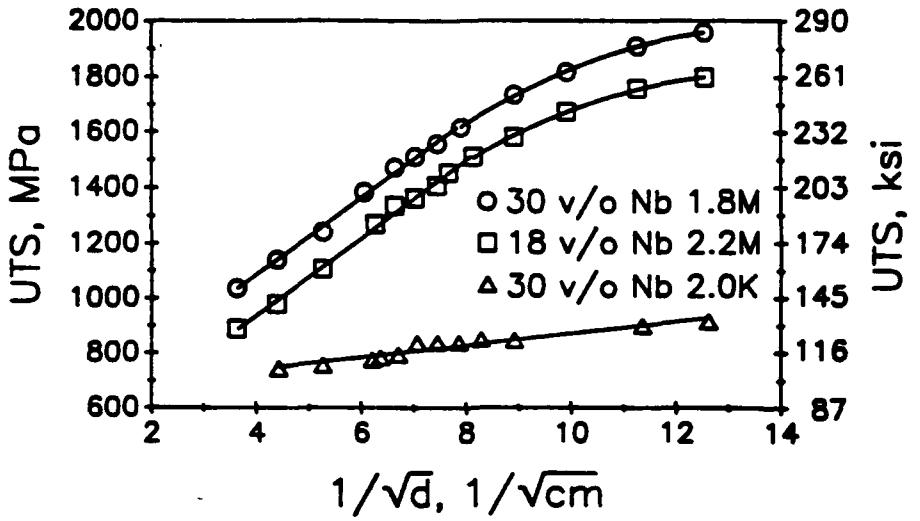

Figure 2. Ultimate tensile strength as a function of root reciprocal wire size for the coarse-filament 2.0K and fine-filament 1.8M and 2.2M Cu-Nb composite wires.

defects. The defects, predominantly crystal lattice distortions called dislocations, act to hinder further deformation of the materials. Heavily deformed materials such as small wires tend to be strong by virtue of their high dislocation densities. In the present case of Cu-Nb composites both the Nb filaments and the Cu matrix are known to experience dramatic rises in dislocation density as the wires are deformed during drawing. The distortion of the microstructure inherent in dislocations acts to disrupt electrical conduction. An indication of the dislocation density in the Cu can be gained by considering the electrical resistivity of the wires. Because of the much higher resistivity of Nb, the normal state conductivity of the wires is governed by the Cu matrix. The dependence of the electrical resistivity on reciprocal wire size is shown in Figure 3. The coarse-filament 2.0K data is fitted by a single straight line indicating that electrical resistivity ρ is given by

$$\rho = \rho_o + \frac{K}{d} .$$

The 1.8M and 2.2M composites have significantly higher resistivities at each wire size. Given its higher Nb volume fraction, it is expected that the resistivity of the 1.8M composite is greater than that of the 2.2M design at each wire size. The fine-filament curves are initially quite linear but become parabolic at the finest wire sizes. The deviations from linearity occur at the same wire sizes as did the bends in the ultimate tensile strength curves. This suggests that the mechanical strengthening is due to the increased dislocation density. The experimental results of Rider and Foxon (12) and the theoretical considerations

of Brown (13) suggest that Cu resistivity is directly proportional to dislocation density with a Cu dislocation resistivity on the order of 2×10^{-19} Ωcm^3. Therefore the dislocation density ρ_{dis} in the linear portion of the Figure 3 curves is given by

$$\rho_{dis} \alpha \frac{K'}{d} .$$

Noting that the dependence of strength σ on dislocation density is given by $\sigma = \sigma_o + K''\sqrt{\rho_{dis}}$ (14), the dependence of strength on wire size becomes

$$\sigma = \sigma_o + \frac{k}{\sqrt{d}} ,$$

which is the Hall-Petch relationship. Thus the strengthening behavior noted in the Cu-Nb composites of this study is consistent with both the spacing of barriers (the Cu matrix-Nb filament interfaces) and the increase in dislocation density (form wire drawing deformation).

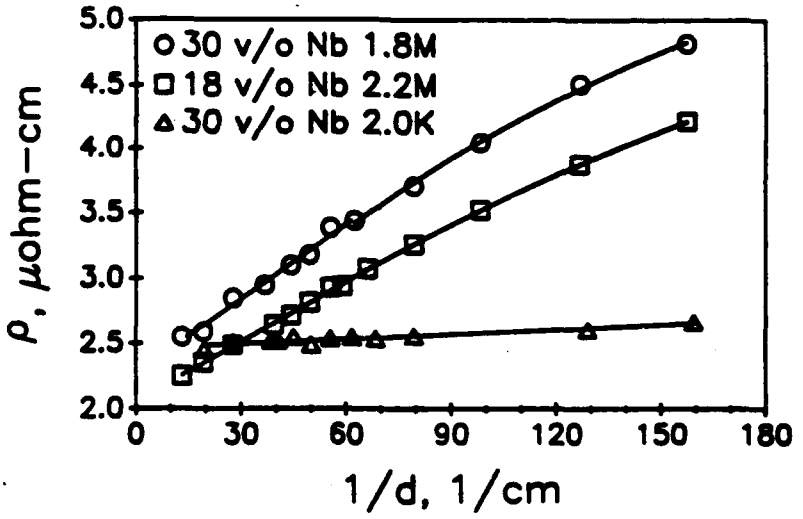

Figure 3. Electrical resistivity as a function of reciprocal wire size for the coarse-filament 2.0K and fine-filament 1.8M and 2.2M Cu-Nb composite wires.

From an applications viewpoint it is the tradeoff between strength and electrical conductivity that is most important. It is important to determine [1] whether fine-filament composites provide a better tradeoff and [2] the impact of volume fraction on the strength-conductivity compromise. These issues are addressed by Figure 4 in which electrical conductivity is plotted as a function of ultimate tensile strength. For each composite conductivity is linear with respect to ultimate tensile strength. The 1.8M and 2.2M fine filament data are described by a single line. Thus, the choice of Nb volume fraction should be

made on the basis of cost, ease of fabrication, and range of applications. The coarse-filament 2.0K composite exhibits an inferior tradeoff. Its properties can be bettered by the fine-filament designs with relatively large interfilament spacings. There is a clear benefit to be obtained by using the fine-filament composites. The choice of interfilament spacing must be made on the specific requirements of each application.

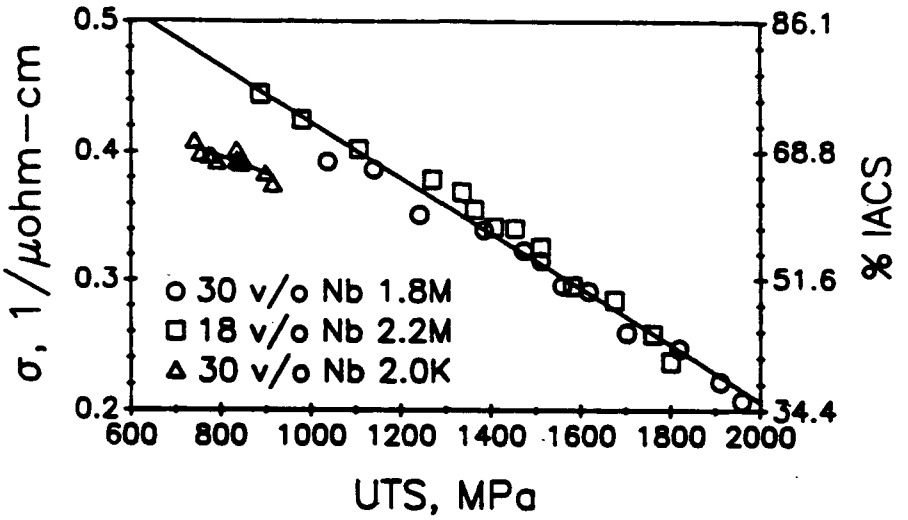

Figure 4. Electrical conductivity as a function of ultimate tensile strength for the coarse-filament 2.0K and fine-filament 1.8M and 2.2M Cu-Nb composite wires.

One of the main concerns in high current applications is loss of strength by annealing. Under certain conditions such as spaceborne applications the limited cooling capability may demand elevated temperature service. Klein and Rose (9) have shown that coarse-filament Cu-Nb composites anneal fully by 400°C. A series of trials were performed to demonstrate the resistance of fine filament composites to strength loss. Samples of the 2.2M composite of various wire sizes were annealed for 1 hr at temperatures of 200 to 700°C. The wires were then tensile tested at room temperature to determine their ultimate tensile strength. The results of these tensile tests are given in Figure 5. One surprising result is that wires annealed at 200°C are marginally stronger that as-drawn wires. This phenomena is a direct result of the thermal induced relief of residual stresses described by Klein and Rose (9). Although some strength loss is evident at temperatures as low as 300°C, even the finest filament wires retain more than 2/3 of their as-drawn strength after annealing at 500°C. Above 500°C the strength advantage of the finest filament wires is largely diminished.

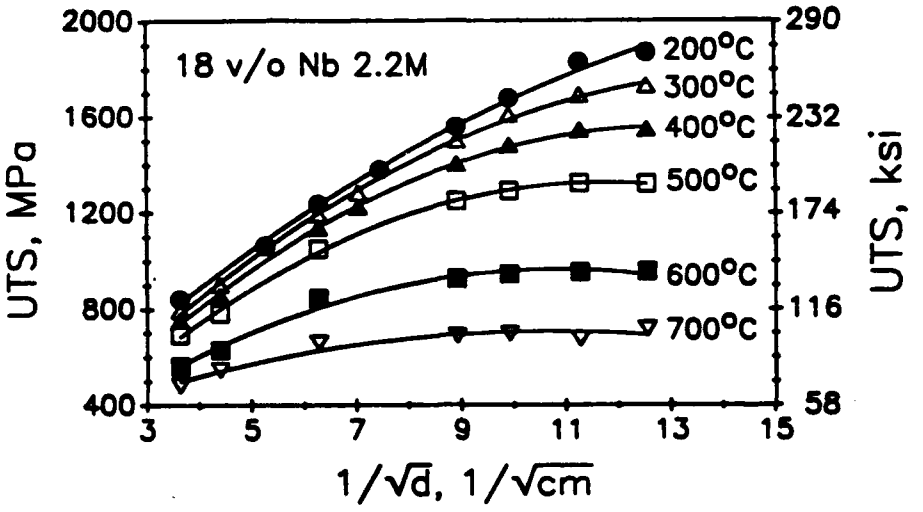

Figure 5. Ultimate tensile strength as a function of root reciprocal wire size for fine-filament 2.2M Cu-Nb composite wires given 1-hr heat treatments at different temperatures.

3.4 CONCLUSIONS.

The strengthening of multifilamentary Cu-Nb composites with decreasing wire size is generally described by a Hall-Petch relationship $\sigma = \sigma_o + k/\sqrt{d}$. It is likely that the strengthening occurs through a combination of interface barriers and dislocation density. The resistivity of wire of different sizes is closely described by $\rho = \rho_o + k/d$. At the smallest sizes of the fine-filament composites the rates of increase in strength and resistivity are somewhat diminished. In considering the tradeoff between electrical conductivity and mechanical strength, the coarse-filament wires are clearly inferior. In the fine-filament wires the strength-conductivity tradeoff is similar over a wide range of Nb volume fraction. All sizes of the fine-filament composites display excellent resistance to annealing at temperatures below 500°C. However, the finest microstructures have relatively little advantage if sustained service at higher temperatures is anticipated.

SECTION 4

ANNEALING BEHAVIOR OF Nb FILAMENTS

4.1 CONCEPT AND APPROACH.

The strength of multifilamentary composites can be degraded by annealing of matrix and/or filament materials. The annealing behavior of Cu-Nb composites is commonly examined by monitoring electrical resistivity. Since Cu is a much better normal state conductor than Nb, room temperature or elevated temperature resistivity cannot reveal thermally induced changes in Nb filaments. Although it is commonly assumed that annealing of the Cu matrix is responsible for strength loss at service temperatures below 500°C, the small size of the Nb filaments suggests that they may also be vulnerable. While Cu is always a normal state conductor, Nb becomes superconducting at very low temperatures. As such, the superconducting properties of Cu-Nb composites are governed by the Nb filaments. Moreover, the superconducting properties of Nb are strongly influenced by its deformation conditions. Therefore, the superconducting properties of Cu-Nb composites given various heat treatments should reveal Nb annealing behavior.

Microfilamentary composites of continuous Nb fibers in Cu matrices were tested for superconducting transport properties after heat treatments at 200 to 900°C. The critical current density at any given applied magnetic field was reduced dramatically as the heat treatment temperature was increased. The scaling relations describing the critical current as a function of applied field shifted from conventional $(1-h)^2$ scaling to higher order relations as the heat treatment history was varied. Critical temperature transitions were abnormally broad in the fine-filament composites examined. The upper critical fields and transition temperatures approached bulk values after severe heat treatment.

4.2 INTRODUCTION.

The effect of heat treatment on the nonsuperconducting electrical properties of multifilamentary Cu-Nb composites has been addressed by several investigations (15,6,9). Since the normal state conductivity of Cu is so much greater than that of Nb, these studies have served largely to indicate the annealing and interfacial scattering behavior of the Cu matrix as constrained by the Nb filaments. Resistivity studies of *in-situ* composites as a function of temperature have been pursued to indicate the annealing behavior of the Cu (15,6). Resistivity and thermal contraction observations of continuous filament Cu-Nb composites have related matrix annealing behavior to the relief of large residual strains introduced during cold drawing to final wire size (9). However, heat treatment at even moderate temperatures can be expected to alter the properties of the small Nb filaments as well as the surrounding Cu matrix. The effects of heat treatment on the Cu and Nb can be partially separated by considering the superconducting behavior of the composites. Since the Cu matrix

is not superconducting the critical current and transition temperature of the composites are governed by the properties of the Nb filaments. The present work on continuous-filament materials produced by stack-and-draw methods describes superconducting behavior in multifilamentary Cu-Nb composites in which there is little chance of filament contamination by matrix Cu during fabrication.

The heat treatment of Cu-Nb composite wires might change the superconducting properties by altering either the Cu matrix or the Nb filaments. Superconducting wires comprised of multifilamentary Nb_3Sn in a bronze matrix respond strongly to their residual stress states at 4.2 K (16,17). Recent experiments show that annealing cold-drawn Cu-Nb composite wires at temperatures as low as 300°C can strongly alter the residual stresses present at room temperature (9). Additionally, the residual stress state of the Nb filaments at 4.2 K will be influenced by the differing thermal contractions of Cu and Nb as well as the possible complication of plastic deformation in an annealed Cu matrix. The effect of heat treatment temperatures up to 900°C on the internal structure of Nb filaments is not well defined. Moderately deformed Nb single crystals have exhibited no thermally activated dislocation motion below 1000°C (18). Although 900°C is less than half the absolute melting point of Nb, the coalescence observed in fine-filament Cu-Nb composites (19,20) indicates that major changes can occur within the Nb fibers at much lower temperatures.

The critical current density, J_c, at an applied magnetic field, H, may be enhanced or degraded as the filament size is decreased. At filament diameters greater than 1 μm it is generally observed that increasing cold work enhances the J_c of Nb (21). Indeed, this trend as well as an adherence to Kramer (22) scaling was indicated in the magnetization experiments of Mathur, Ashkin, and Deis (23) for Cu-Nb composites having filament diameters of 7 to 18 μm. However, the quadruple extrusion composites of Cline, Strauss, Rose, and Wulff (24) exhibited a decrease in J_c as the filament size was taken below 160 nm. This suggests that alternative scaling relations may be required to describe flux pinning in these materials. The present study defines Nb filament properties as a function of annealing history by examining the transport and critical temperature behavior of coarse-filament and fine-filament Cu-Nb composites given heat treatments at 200 to 900°C.

4.3 EXPERIMENT.

The continuous filament composites of this study were fabricated by the Levi process as applied to Cu-Nb composites by Cline, Strauss, Rose, and Wulff (25). In this method OFHC Cu tubes are first swaged and drawn onto Nb rods. The resulting monofilament composite is then hex-drawn and cut into segments so that a billet can be assembled by stacking numerous hexes inside a Cu pipe. After the billet is evacuated and welded shut, extrusion and drawing operations are employed to reduce the composite to final wire size. Finer fila-

ment sizes can be achieved if additional bundling, extrusion, and reduction cycles are performed. Two composites designs were used in this investigation. The "2.0K" composite is a single extrusion design possessing 1956 filaments of 3.1 μm nominal diameter at a 0.0254 cm diameter wire size. The "1.8M" composite is a double extrusion design utilizing 709 colonies of 2479 filaments each to give 1.76 million filaments of 0.11 μm nominal diameter at a 0.0267 cm wire diameter.

The dependence of critical current density on applied magnetic field was measured to ascertain the effects of both fine-filament structure and heat treatment on the superconducting properties of Cu-Nb composites. The measurements were performed at 4.2 K with a four-point probe arrangement. The usual 1μV/cm transition criterion was used for samples placed in a magnetic field provided by a NbTi superconducting magnet. Most wires were tested at a nominal diameter of 0.026 cm in a transverse field through a current density range of 10^2 to 10^5 amps/cm^2. In all cases the field was set before sweeping the current to obtain a transition.

The critical temperatures of 0.026 cm diameter composites were determined resistively. The specimens were attached to a jig containing a germanium cryothermometer by four solder contacts. The jig was then inserted into a Cu can wound non-inductively with resistance wire. Placement of the can and jig assembly in a 25 mm quartz tube allowed evacuation by a mechanical pump prior to the introduction of a small quantity of He transfer gas. After immersion and equilibration of the tube in liquid He, currents were applied to the sample and thermometer. Power was then applied to the heater can to gradually drive the sample through its transition. An overall sample current density of 30 amps/cm^2 was chosen to provide a better comparison with the critical current measurements.

4.4 RESULTS AND DISCUSSION.

The superconducting properties of 0.026 cm diameter 2.0K and 1.8M Cu-Nb wires were determined in the as-drawn condition as well as after two hour heat treatments performed in a vacuum of better than 2 x 10^{-6} Torr at temperatures ranging from 200 to 900°C. The overall critical current densities as a function of applied field, J_c *vs.* H, for the 1.8M composite are shown in Figure 6. As the annealing temperature rises toward 700°C the critical current capacity degrades monotonically. The curves for samples heat treated at 701°C and 798°C are essentially the same whereas a distinctly different character is exhibited by the sample heat treated at the highest temperature.

The determination of the scaling laws appropriate to the 1.8M data would allow the definition of the upper critical field H_{c_2} effective over the critical current regime investigated. The shape of the as-drawn 1.8M J_c *vs.* H curve implies

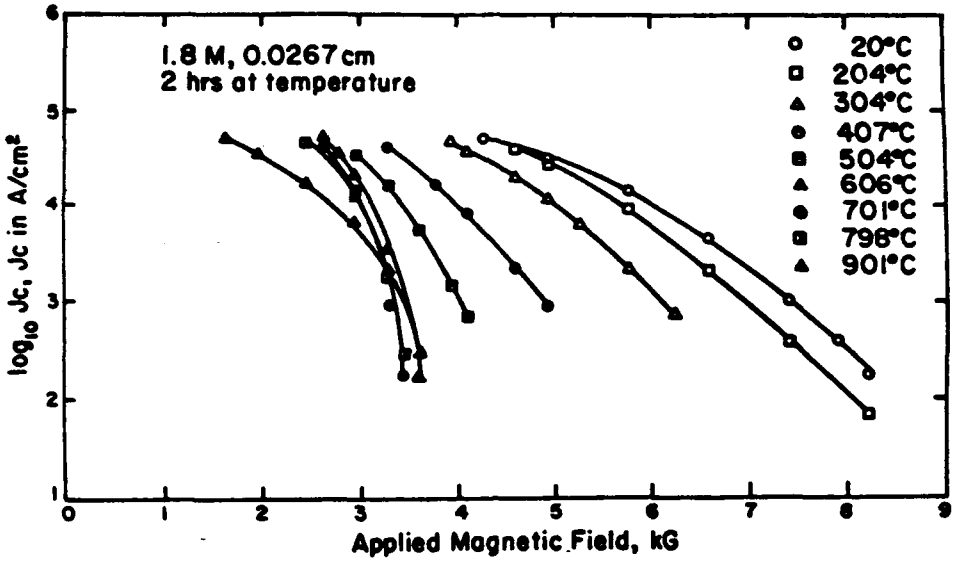

Figure 6. Logarithm of the critical current density (overall J_c in amps/cm^2) as a function of applied magnetic field for fine-filament 1.8M Cu-Nb composites subjected to 2-hour heat treatments at various temperatures.

a rapid reduction of the critical current density as the reduced field $h = H/H_{c_2}$ is increased. As in the case of fine-filament Nb_3Sn data (26), it was found that such behavior failed to fit the Kramer (27) scaling law

$$F_p = J_c' H = K_s \sqrt{h}\,(1-h)^2 .$$

Here, F_p is the flux pinning force density, J_c' is the critical current density in the filaments and K_s is a constant for a given sample and temperature. The associated $(1-h)^2$ extrapolation function for H_{c_2} is

$$\sqrt{J_c'\sqrt{H}} = \left(1-\frac{H}{H_{c_2}}\right)\sqrt{\frac{K_s}{\sqrt{H_{c_2}}}} .$$

The higher order $(1-h)^4$ scaling law employed successfully for the fine-filament Nb_3Sn data is

$$F_p = J_c' H = K \sqrt{h}\,(1-h)^4 .$$

The corresponding higher order extrapolation function becomes

$$\sqrt[4]{J_c'\sqrt{H}} = \left(1-\frac{H}{H_{c_2}}\right)\sqrt[4]{\frac{K}{\sqrt{H_{c_2}}}} .$$

As can be seen in Figure 7 the $(1-h)^4$ scaling is much more appropriate than the $(1-h)^2$ relation for the as-drawn 1.8M wire. Note the linearity of the H_{c2} extrapolation function as it indicates an upper critical field of 9.55 kG. The failure of the more common $(1-h)^2$ relation in describing the critical current behavior of as-drawn Cu-Nb wires is not surprising. As noted in a discussion of Nb_3Sn flux pinning by Evetts and Plummer (28), there exist serious reservations concerning the applicability of Kramer scaling relations to highly distorted structures. The cold work introduced by drawing to final wire diameter without intermediate anneals will produce a high defect density in the Nb filaments. Only after severe annealing will the internal structure of the Nb become more consistent with the assumptions of the model.

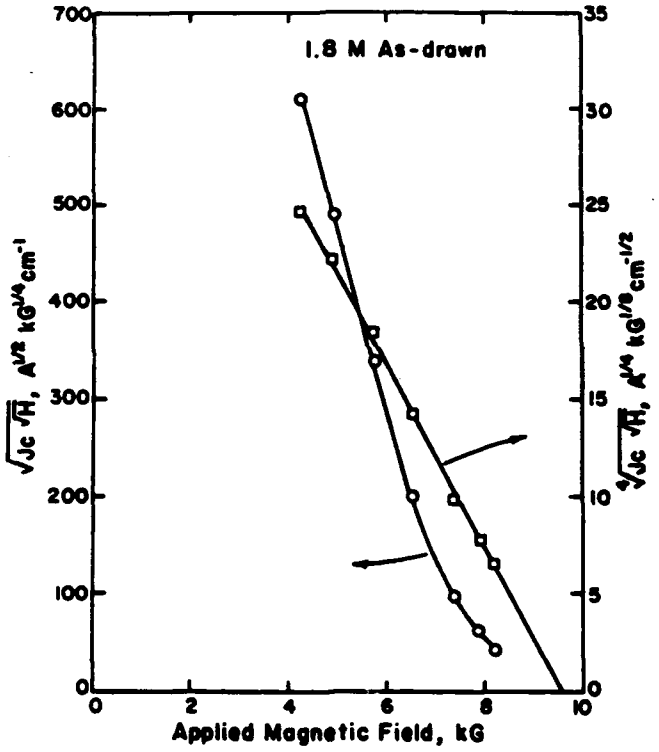

Figure 7. Determination of H_{c2} by extrapolation of $\sqrt{J_c\sqrt{H}}$ or $\sqrt[4]{J_c\sqrt{H}}$ to the applied field axis. Linearity implies that $(1-h)^4$ scaling is appropriate for this 1.8M as-drawn sample.

The appropriate scaling relation for the 1.8M composites changes at heat treatment temperatures above 650°C. The 798 and 901°C data conform strongly to $(1-h)^2$ scaling. Plots employed for the H_{c2} determination for the 901°C sample are shown in Figure 8. The J_c *vs.* H data of this sample conforms closely to the $(1-h)^2$ scaling relation. Similar results hold for the 798°C sample whereas the 701°C sample conforms to either type of scaling only moderately well. A

summary of the scaling parameters of the 0.0267 cm 1.8M composite wires is given in Table 2. Further reductions in the 1.8M wire diameter resulted in a loss of critical current capacity. As indicated in Table 3 the as-drawn wires continued to conform to the higher order $(1-k)^4$ scaling. However, the degradation in J_c with decreasing wire size was reflected not only in a reduction of H_{c_2}, but also in declining values of the slope of the extrapolation plots.

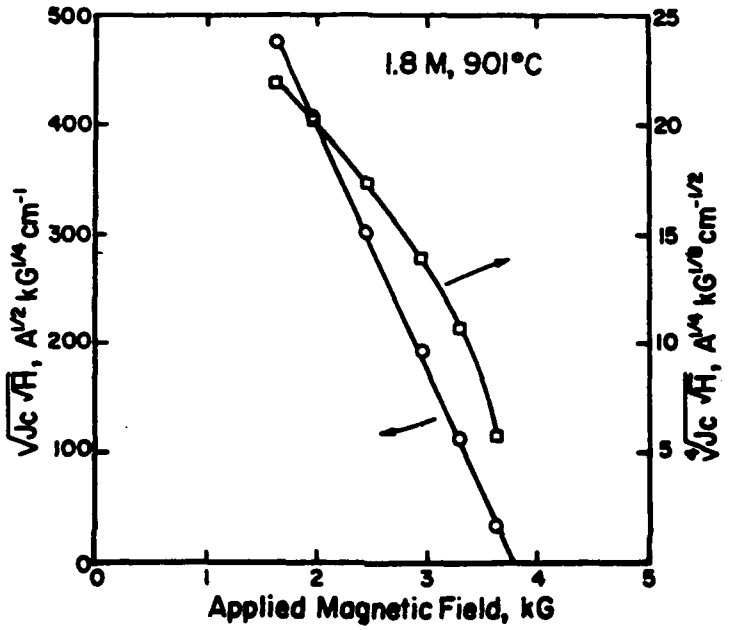

Figure 8. Determination of H_{c_2} by extrapolation of $\sqrt{J_c\sqrt{H}}$ or $\sqrt[4]{J_c\sqrt{H}}$ to the applied field axis. Linearity implies that $(1-k)^2$ scaling is appropriate for this 1.8M sample heat treated at 901°C for 2 hours.

The overall critical current as a function of applied field results for the coarse-filament 2.0K composite are only qualitatively similar to those described above. The J_c *vs.* H characteristics of 0.0254 cm diameter 2.0K wires given 2-hour heat treatments up to 900°C are shown in Figure 9. At any given heat treatment condition the critical current capacity of the 2.0K wires is inferior to that exhibited by their 1.8M counterparts. The scaling behavior of the coarse-filament 2.0K composites is initially quite different than that shown by the fine-filament wires. The critical current behavior of 2.0K wires in the as-drawn condition and those annealed at temperatures below 450°C is such that the plot of $\log_{10}J_c$ *vs.* H is linear over the current density range investigated. Intermediate heat treatment temperatures result in J_c *vs.* H behavior that can be represented by the $(1-k)^4$ scaling discussed above. As before, the highest heat treatment temperatures yield curves that are consistent with $(1-k)^2$ scaling.

Table 2. Values of H_{c_2} derived from fitting the 0.0267 cm 1.8M J_c *vs.* H data to $(1-h)^2$ or $(1-h)^4$ scaling.

Temperature of 2-hour anneal (°C)	n to fit $F_p = K_o\sqrt{h}(1-h)^n$	Correlation Coefficient of fit	H_{c_2} (kG)
as-drawn	4	0.9992	9.55
204	4	0.9953	9.01
304	4	0.9993	7.55
407	4	0.9994	6.02
504	4	0.9996	4.84
606	4	0.9985	4.00
701	4	0.9951	3.73
798	2	0.9994	3.53
901	2	0.9996	3.79

Table 3. Values of H_{c_2} derived from fitting J_c *vs.* H data of as-drawn 1.8M wires of various diameters to $(1-h)^4$ scaling.

Wire diameter (cm)	n to fit $F_p = K_o\sqrt{h}(1-h)^n$	Correlation Coefficient of fit	H_{c_2} (kG)
0.0267	4	0.9974	9.67
0.0208	4	0.9988	9.01
0.0170	4	0.9980	8.20
0.0135	4	0.9949	6.67

This allowed the effective upper field to be determined readily for wires given heat treatments above 450°C. For the wires given less severe heat treatments the upper critical field was estimated as the applied field that would allow an overall critical current density of 10 amps/cm^2. This is consistent with the H_{c_2} values obtained from application of the scaling laws to the other wires in the sense that extrapolation of their curves gives H_{c_2} as the applied field at this current density. The scaling characteristics of the 2.0K wires are noted in Table 4. The data indicate that H_{c_2} falls sharply as the heat treatment temperature is raised toward 650°C. As was the case with the 1.8M composite, heat treatment of the 2.0K wires above 650°C resulted in a limiting value of 3.6 kG for the upper critical field.

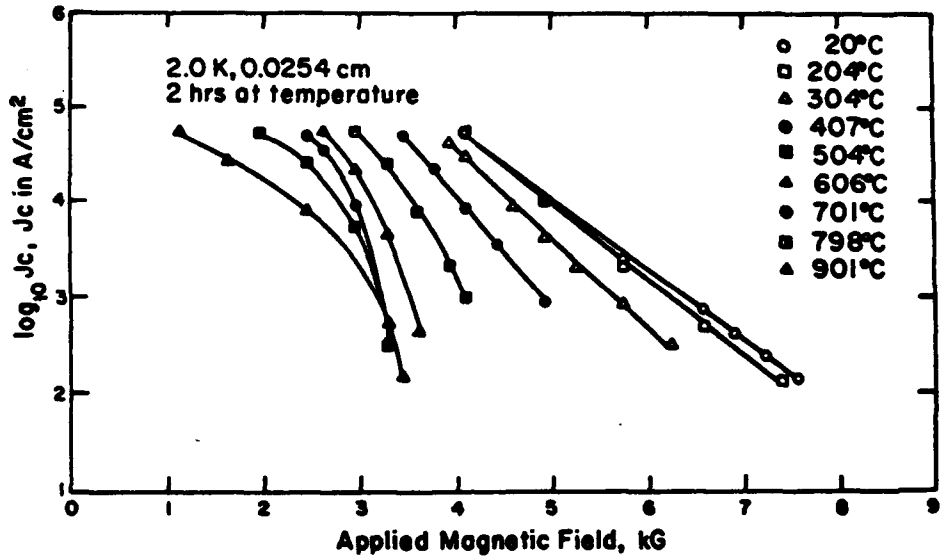

Figure 9. Logarithm of the critical current density (overall J_c in amps/cm^2) as a function of applied magnetic field for coarse-filament 2.0K Cu-Nb composites subjected to 2-hour heat treatments at various temperatures.

Table 4. Values of H_{c_2} derived from fitting the 0.0254 cm 2.0K J_c *vs.* H data to $(1-h)^2$ or $(1-h)^1$ scaling.

Temperature of 2-hour anneal (°C)	n to fit $F_p = K_o\sqrt{h}(1-h)^n$	Correlation Coefficient of fit	H_{c_2} (kG)
as-drawn	[a]	[a]	9.1
204	[a]	[a]	8.7
304	[a]	[a]	7.8
407	[a]	[a]	6.6
504	4	0.9995	4.79
606	4	0.9982	4.07
701	2	0.9974	3.37
798	2	0.9961	3.45
901	2	0.9992	3.61

[a] The $\log_{10} J_c$ *vs.* H plot is linear for these samples.

The critical temperature T_c of a superconductor is often taken as an indicator of the quality of the material. As a comparison, a Nb single crystal tested at a current density of 3.0 amps/cm^2 was found to have a relatively sharp superconducting transition starting at 9.15 K and ending at 9.12 K. The 30 amps/cm^2 T_c results for the 1.8M and 2.0K composite wires appear in Figure 10. Under all heat treatment conditions examined the transitions for the 2.0K wires are relatively sharp (< 0.09 K wide) with the transitions occurring in the vicinity of 9 K. Samples of the 2.0K composite given two-hour heat treatments at temperatures below 400°C have slightly broadened transitions. Also notable is a significant depression and broadening in the superconducting transitions of samples heat treated above 750°C. The characteristics of the critical temperature transitions of the 1.8M wires are remarkably different. Under all but the most severe heat treatment conditions the transitions are quite broad and appreciably depressed. The effect of heat treatment at temperatures below 600°C is to depress the transition temperature while maintaining the breadth of the transition. Heat treatments above 600°C tend to increase T_c and sharpen the transition.

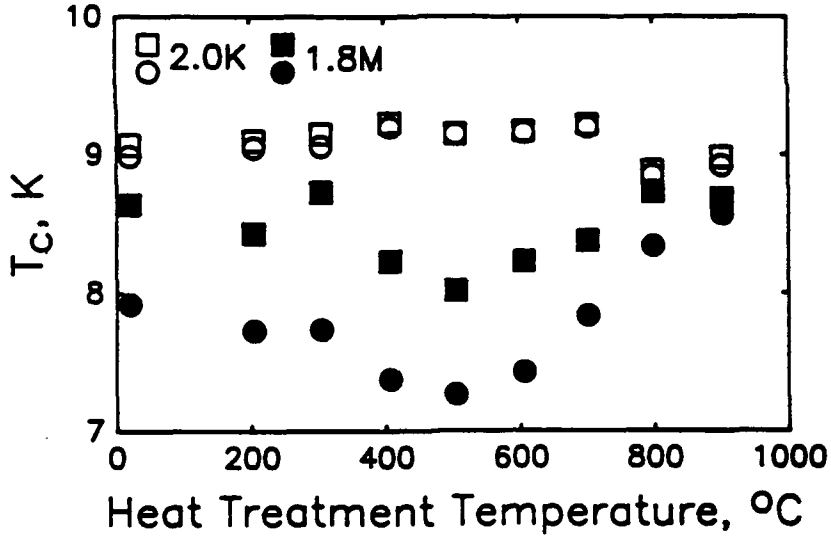

Figure 10. Critical temperature as a function of 2-hour heat treatment temperature for 0.0257 cm 2.0K and 0.0267 cm 1.8M Cu-Nb composite wires. Squares and circles denote the onsets and completions of the transition to the superconducting state, respectively.

4.5 CONCLUSIONS.

The critical current capacity of cold-drawn Cu-Nb multifilamentary composites is significantly reduced by heat treatment at temperatures as low as 200°C. Application of the appropriate scaling laws to the coarse-filament 2.0K and fine-filament 1.8M data indicates that the reduction is largely the result of a depression of the effective upper critical field. Shown in Figure 11 are the effective H_{c_2}'s governing the critical current behavior of the two composites in the range of 100 to 10^5 amps/cm^2. As the heat treatment temperature was raised from 200 to 600°C H_{c_2} was reduced by more than 1 kG for each 100°C. Heat treatment at temperatures above 650°C allowed the upper critical field to reach a limiting value of about 3.4 to 3.5 kG with some recovery of H_{c_2} after annealing at 900°C. In addition, the critical current behavior of the 1.8M wires subjected to heat treatments above 750°C conformed to the more usual $(1-k)^2$ scaling.

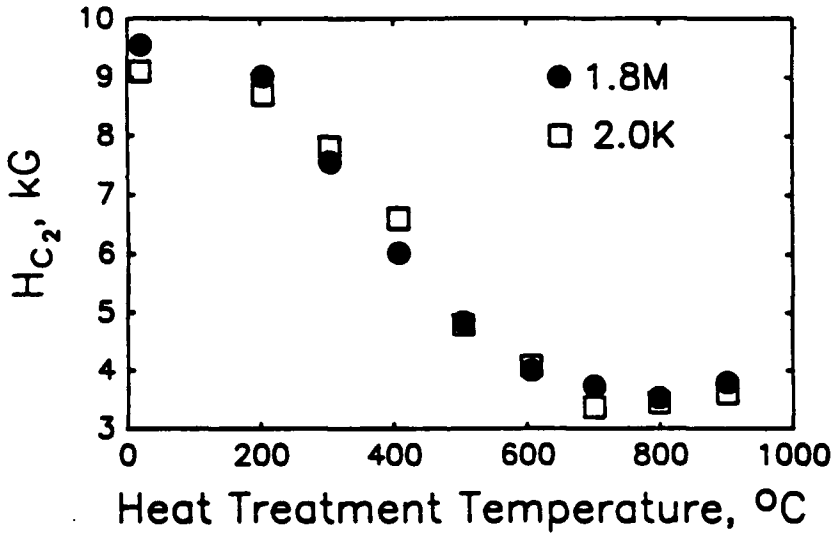

Figure 11. The effective upper critical field of 0.026 cm 2.0K and 1.8M wires as a function of heat treatment temperature.

The observed changes in H_{c_2} upon annealing would seem to result from a combination of stress relief, recovery processes, and filament coalescence. Stress effects can explain much of the critical current behavior in wires given low temperature heat treatments. The higher tensile strength and lower volume fraction of the Nb filaments as compared to the Cu matrix allows high residual tensile strains to be introduced in the filaments during cold drawing to final wire size. Differential thermal expansion experiments have shown that the Nb filaments in the present 0.026 cm diameter composites have residual

tensile strains of 0.4 to 0.75 percent at room temperature.[3] In the as-drawn wires the tensile stress in the Nb filaments is balanced by compressive stress in the matrix Cu. However, since there is much more Cu than Nb in these composites, the residual compressive stresses in the Cu matrix are of much smaller magnitude than the tensile stresses in the Nb filaments. The higher residual strain levels are associated with the fine-filament 1.8M composite because the greater cold work and smaller interfilament spacings in the fine filament materials produce a stronger Cu matrix. The effect of heat treatment is to relieve the residual strains by the relatively low temperature annealing of the Cu matrix. Resistivity studies of these composites have shown that 0.026 cm diameter 2.0K wires are fully annealed by heat treatments at less than 500°C. Fine-filament 1.8M wires of similar diameter experience significant decreases in resistivity beyond 600°C.[3]

The stress state of the Nb filaments is particularly important to the critical current behavior of Cu-Nb composites. The application of tensile strains to as-drawn or heat treated Cu-Nb composites can drastically enhance the critical current capacity at 4.2 K according to

$$\log_{10} J_c = m\,\varepsilon + b$$

where ε is the applied strain and m and b are constants for a given sample, applied magnetic field, and temperature conditions (29). An applied strain of 1 % often increases the critical current capacity by more than an order of magnitude. This suggests that the effect of the low temperature heat treatments of this investigation is to relieve the residual tensile strains in the filaments of the as-drawn wires by permitting relaxation and annealing of the matrix Cu. The lower strain in the Nb filaments results in reduced critical current capacity without internal structural changes in the filaments. This apparent reduction in the upper critical field with reduced filament tension is consistent with the observations of Hill and Rose (30) and Klein (26).

The present experimental results indicate that heat treatments performed above 400°C alter the internal structure of the Nb filaments. The Cu matrix of the coarse-filament 2.0K composite will be fully annealed by heat treatments at 450°C. However, the H_{c2} values shown in Figure 11 are still decreasing between 500 and 800°C. In addition, the 2.0K critical temperature transitions described by Figure 10 are sharpest between 500 and 700°C. Similarly, the sharpness and midpoint temperature of the 1.8M superconducting transitions increase with increasing annealing temperature above 500°C. Microscopic examination of the fine-filament 1.8M composite reveals that high temperature heat treatments cause the closely spaced filaments to coalesce as shown in Figure 12. Coalescence of the 1.8M fine-filament colonies would result in large porous "filaments" similar in size to the filaments of the 2.0K composite. This is indicated by the agreement of the 1.8M and 2.0K J_c vs. H, H_{c2}, and T_c behavior in wires heat treated above 550°C. The action of rapid Nb recovery processes is further supported by electron microscopy of *in-situ* Cu-Nb composites. Verhoeven, Downing, Chumbley, and Gibson have observed the onset of Nb filament coars-

ening at temperatures as low as 320°C in fine-filament *in-situ* composites (15). The functional dependence of the critical current on the applied field is determined by the defect structure responsible for flux pinning. Although $(1-h)^2$ scaling is appropriate for wires possessing well annealed Nb filaments, other relations such as the $(1-h)^4$ scaling noted in this investigation are necessary to describe flux pinning behavior in heavily deformed Nb.

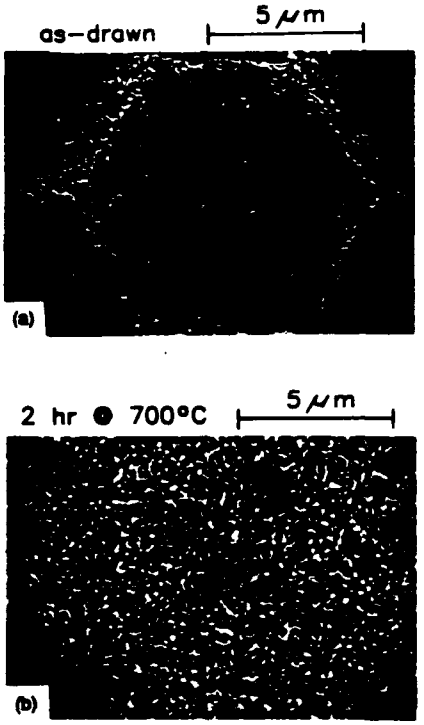

Figure 12. Cross-sections of representative colonies of the 1.8M double extrusion composite are shown (a) in the as-drawn condition and (b) after a two hour heat treatment at 700°C. Heat treatment has caused the 2479 Nb filaments of the as-drawn colony to coalesce into a sponge-like structure. The matrix Cu has been etched away to reveal the Nb morphology.

SECTION 5

PULSED CURRENT FATIGUE OF Cu-Nb COMPOSITES

5.1 CONCEPT AND APPROACH.

The suitability of multifilamentary composites of continuous Nb fibers in Cu matrices for high stress conductors in pulsed current applications was assessed by a novel electromechanical testing method described as pulsed current fatigue. In this technique direct current pulses are applied to a vertically oriented wire supporting a dead weight. Expansion resulting from joule heating during the pulse and contraction due to convective and radiative cooling between pulses causes periodic mechanical loading of the wire during the pulsed current cycling. Plots of fracture stress as a function of logarithm of number of cycles or time serve to define the role of current level, pulse duration, and pulse frequency on the pulsed current life of composite conductors. Fine-filament Cu-Nb composites exhibit pulsed current fatigue performance that is markedly superior to that observed in corresponding coarse-filament materials.

5.2 INTRODUCTION.

Many pulsed current applications require high strength, high conductivity electrical conductors. Projected pulse power requirements include currents in the range of kiloamps to megaamps, repetition rates up to 100 Hz, and pulse widths of 100 nanoseconds to 100 milliseconds (31). Appreciable stresses may arise from Lorentz forces within coiled conductors or from post-pulse recoil effects. Weight and volume restrictions inherent in space and airborne systems place a high priority on mechanically strong conductor materials. The pulsed current fatigue method of conductor testing is intended to combine the mechanical and thermal trauma that a conductor material might experience in a pulsed current system. Although the operating environment and service protocol of implemented pulsed current conductors will be dictated by their specific applications, an experimental method was desired to discriminate between good and poor conductor materials. A conductor exhibiting superior pulsed current fatigue behavior will possess a favorable combination of electrical conductivity, mechanical strength, and resistance to annealing.

Fine-filament Cu-matrix composites are particularly appealing for pulsed current applications because of their high tensile strengths, appreciable resistance to annealing, and electrical conductivities approaching that of pure copper. The strength relationships, annealing characteristics, and elastic modulus of multifilamentary composites have been determined in a number of Cu-matrix systems such as Cu-W (2), Cu-Ag (3,4), and Cu-Nb (5-7). However, most studies of fine-filament composites have been performed on materials fabricated by *in-situ* methods (3-7) to facilitate the preparation of fine filament sizes. The strengths of large filament designs tend to obey the rule of mixtures

(2), whereas the tensile properties of fine-filament composites often exceed linear combination predictions by large margins in both fcc-fcc (4) and fcc-bcc (7) systems. The effect of heat treatment on the nonsuperconducting electrical properties of multifilamentary Cu-Nb composites has been addressed by several investigations (6,9,15). Since the normal state conductivity of Cu is so much greater than that of Nb, these studies have served largely to indicate the annealing and interfacial scattering behavior of the Cu matrix as constrained by the Nb filaments. Resistivity and thermal contraction observations of continuous filament Cu-Nb composites have related matrix annealing behavior to the relief of large residual strains introduced during cold drawing to final wire size (9). However, heat treatment at even moderate temperatures can be expected to alter the properties of the small Nb filaments as well as the surrounding Cu matrix. The effects of heat treatment on the Cu and Nb were largely separated by considering the superconducting behavior of the composites. Klein and Rose (32) have shown that fine Nb filaments anneal significantly at temperatures below 400°C. The present work on continuous-filament materials produced by stack-and-draw methods describes pulsed current fatigue performance of coarse-filament (3 μm diameter) and fine-filament (<0.15 μm nominal diameter) Cu-Nb composites.

5.3 EXPERIMENT.

Pulsed current fatigue is a materials testing technique in which periodic thermal and mechanical loading of a wire specimen is achieved through the application of a pulsed current. The ease with which pulsed current fatigue is implemented can be appreciated by considering the experimental setup shown in Figure 13. The system is designed to apply an axial load to a wire through which current pulses are passed. The wire sample is held vertically between the upper and lower grips. In practice it has proven convenient to fit the upper grip rigidly to the upper crosshead of a tensile testing loadframe. The lower grip assembly is comprised of a wire grip, a weight can, and a rod terminated with a displacement transducer core. The body of the linear variable displacement transformer (LVDT) transducer is mounted onto the fixed crosshead of the tensile loadframe. The LVDT allows thermally and mechanically induced length changes to be monitored during testing. Current flow through the sample is controlled by a specially fabricated pulser circuit. During each cycle the pulser supplies a preset direct current for a short time interval, typically 10 msec, and no current for the rest of the period. The reference frequency supplied by the function generator determines the repetition rate at which the current supplied by the lead-acid battery is applied. An oscilloscope and digital recorder are used to monitor the current pulsing and length fluctuations simultaneously.

Application of a cyclic pulsed current to the sample changes both the temperature and stress state of the wire. Due to the high current densities employed, each pulse causes appreciable joule heating in the current-on portion of the pulse. During the first few cycles there is little heat dissipation

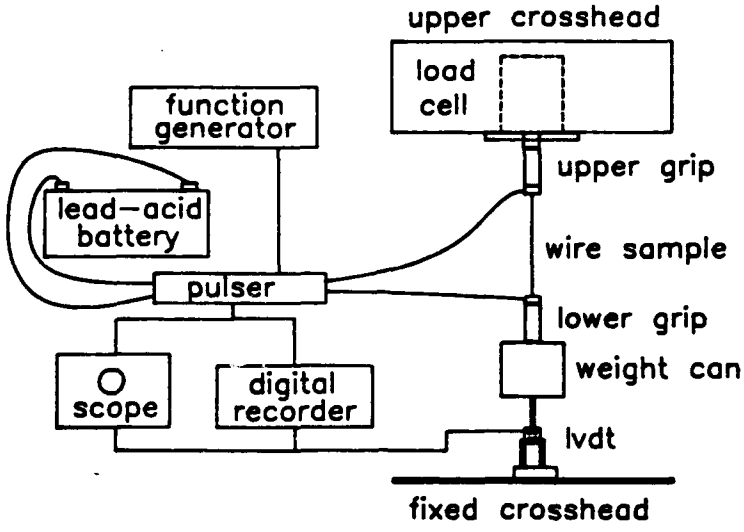

Figure 13. A schematic diagram of the experimental setup for pulsed current fatigue testing.

between the pulses because the wire temperature is only slightly higher than the ambient room temperature. As the wire sample heats, convective and radiation heat transfer increase until the temperature rise during the current pulse is balanced by the temperature drop between pulses. However, even after a large number of cycles the thermal expansion and contraction during a pulse period cause the wire to raise and lower the load resulting from the mass of the lower grip-weight can assembly. Therefore, superimposed upon thermal cycling of the wires is a periodic mechanical loading of the same excitation frequency, that of the pulsed current. The combined thermal and stress cycling under the influence of the current pulses leads to a significant reduction in load carrying capacity of the wires.

The cyclic history of a wire during pulsed current fatigue can be appreciated by considering its temperature and stress state as a function of time. The limited travel of the displacement transducer precludes following the length changes of a wire during warm-up to steady state conditions. However, numerical modeling of pulsed current fatigue allows a complete history to be calculated. Shown in Figure 14 are the calculated curves for temperature and stress during 20 amp, 10 msec, 10 Hz pulsed current fatigue of a 0.0267 cm diameter 30 volume % Nb composite supporting a mass of 1.8 kg. Each pulse causes appreciable heating of the wire, the effect being more pronounced at longer times due to the increase of wire resistivity with increasing temperature. However, since the rate of heat dissipation increases rapidly with rising temperature the average temperature over a cycle asymptotically approaches a steady state value. The axial stress in the wire is determined by a combination of the pulsing conditions, the lower grip assembly mass, and the composite wire's mechanical properties. The application of each current pulse changes

the free (unladen) length of the wire in response to the temperature rise. The resulting raising and lowering of the dead weight provides a mechanical disturbance that initiates vibration of the wire-weight-can combination as a spring-mass system. For example, in Figure 14 there are more than two stress oscillations for each current pulse. That is, the lower grip assembly "bounces" twice before the next current pulse disturbs the motion. Careful examination reveals that there is observable attenuation in the amplitude of the second bounce. Such damping characteristics are more evident under pulse conditions causing more severe mechanical loading.

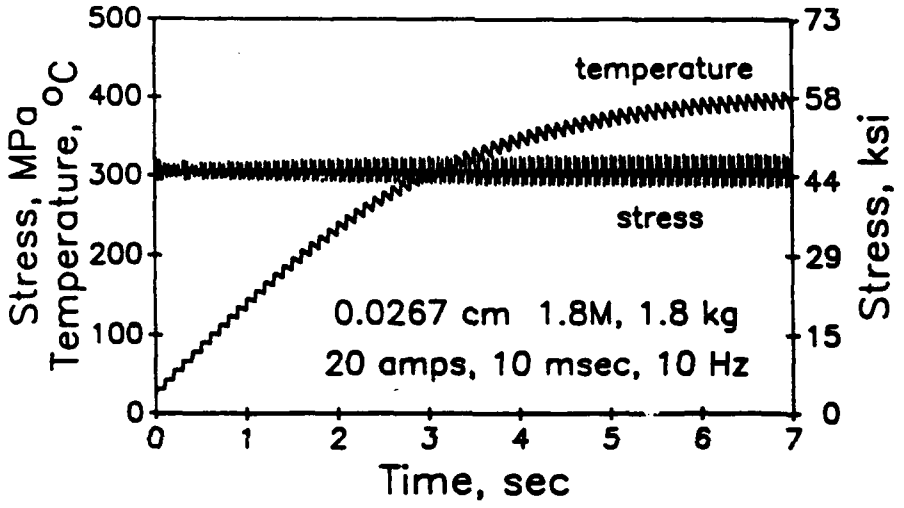

Figure 14. The calculated thermal and stress history of a wire subjected to pulsed current fatigue. The parameters of the numerical simulation model were set to describe 20 amp, 10 msec, 10 Hz pulsing of a 0.0267 cm 1.8M composite supporting a mass of 1.8 kg.

The interaction of the wire length oscillations with the applied current pulse is best appreciated by examining the changes in wire length as a function of time. Shown in Figure 15a are calculated and experimental curves for wire length as a function of time at steady state conditions. In this case a lower grip assembly mass of 0.91 kg was used to load a 0.018 cm wire under 30 amp, 20 msec, and 0.75 Hz pulse conditions. The only adjustment of the model required to match the shapes of the experimental and model length curves was the addition of a damping factor to account for the attenuation of the oscillations. These pulse conditions are particularly severe in that they cause a temperature rise of approximately 300°C during each pulse. This would result in an unladen length increase of approximately 0.74 mm during the current-on interval. However, when the current pulse ends the lower grip assembly is still falling. The cooling wire must therefore arrest the downward motion of the load mass. This causes a jerk on the sample wire that excites sinusoidal oscillations of the wire-lower grip spring-mass system. The combination of the

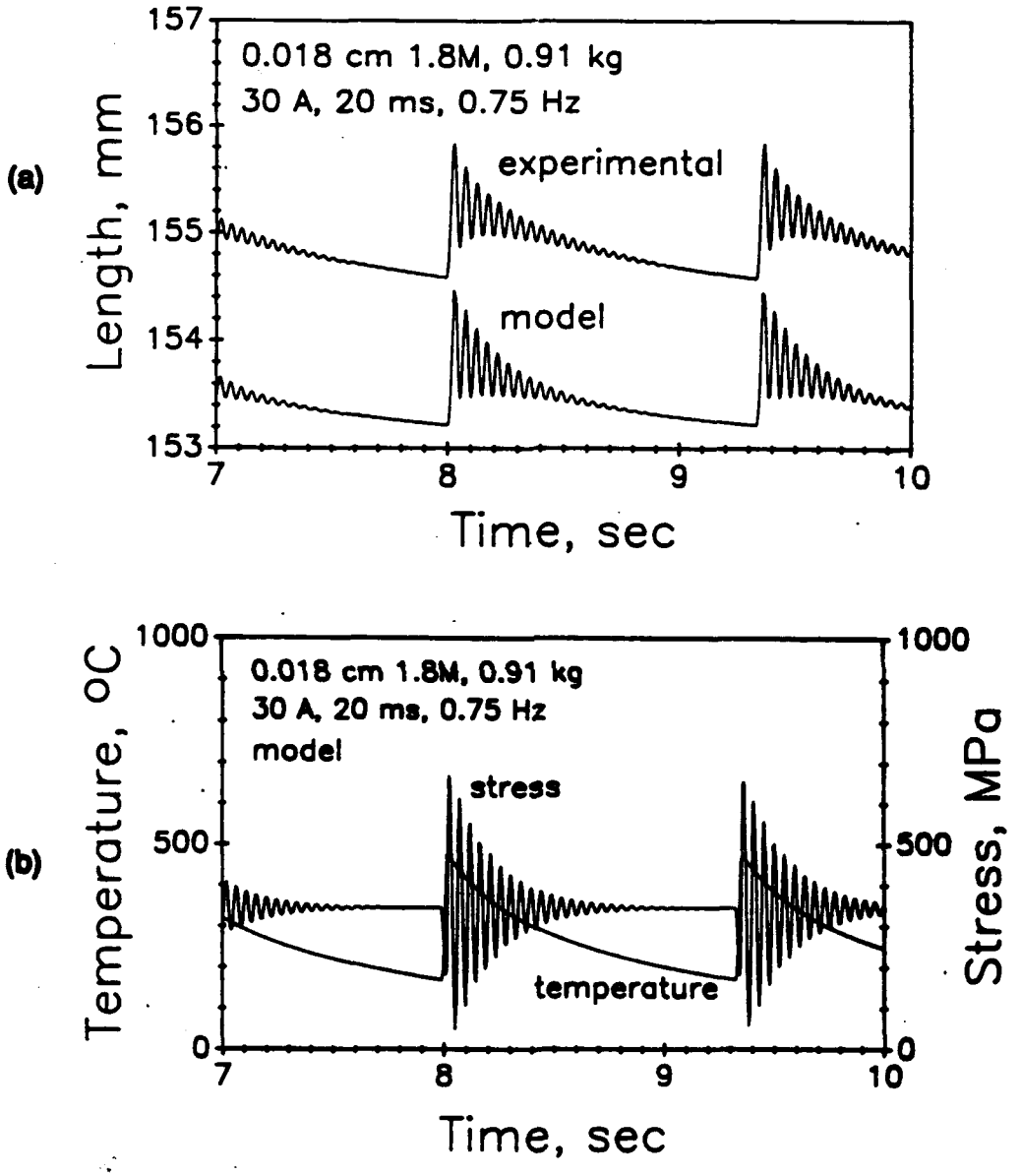

Figure 15. The mechanically severe 30 amp, 20 msec, 0.75 Hz pulse conditions applied to a 0.018 cm 1.8M wire cause a) steady state oscillations of the wire length corresponding to b) large temperature and stress fluctuations as a function of time.

thermal expansion and the jerk result in a laden length change of more than 1.2 mm under these pulse-load mass conditions. Naturally, the severity of this jerk is reflected in the stress history. The length and stress values depicted in Figure 15b were produced by the numerical simulation used to generate the model length trace shown in Figure 15a. Close examination of the stress curve reveals that the initial drop in stress associated with the current-on thermal expansion is followed by a sharp increase associated with arresting the downward motion of the load mass. The peak-to-peak amplitude of the stress oscillations, 620 MPa, is more than 1.8 times the mean stress of 340 MPa. Under these conditions the stress ranges from 670 MPa to 50 MPa during each pulse period. Note also that the time of maximum tensile stress is nearly coincident with the time of maximum temperature. Since increases in the severity of the pulse will raise both the peak temperature and the peak tensile stress, conductor life should be remarkably sensitive to pulse conditions.

5.4 RESULTS AND DISCUSSION.

The pulsed current fatigue method of conductor evaluation was devised to assess the relative performance of candidate high strength electrical conductors in pulsed current applications. The variables inherent in pulsed current fatigue testing can be separated into conductor parameters and current pulsing characteristics. The ability of the test to discriminate between candidate conductors is demonstrated by examining the relative performance of two composite wire designs differing mainly in filament size. The sensitivity of a conductor to the severity of a current pulse was examined by applying pulse conditions of similar average power but different pulse energy to the better conductor.

5.4.1 Filament Size Effects.

The coarse-filament 2.0K Cu-Nb composite was considered as a medium strength material obeying the rule of mixtures with respect to both mechanical and electrical properties. At room temperature a 0.0254 cm 2.0K wire has an electrical resistivity of 2.47 μohm-cm, a yield strength of 525 MPa (76 ksi), an ultimate tensile strength of 785 MPa (114 ksi), and an elongation of 4.0 % over a 10 cm gage length. Since high performance applications are of particular interest, relatively large currents were applied to small wires. The pulsed current fatigue behavior of the 0.0254 cm 2.0K composite wires was determined with 10 msec, 10 Hz direct current pulses. The 15 and 20 amp current levels employed correspond to overall current densities of 3×10^4 and 4×10^4 amps/cm^2, respectively. As is usually the case with materials exposed to cyclic trauma the number of cycles to failure is strongly dependent on the stress levels employed. Representation of all the data on a single graph requires semilog axes as shown in Figure 16. The vertical axis is the static stress obtained by dividing the weight of the lower grip assembly by the cross-sectional area of the wire. The horizontal axis is the number of pulse cycles to failure plotted according to logarithmic graduations. The 15 and 20 amp curves have similar shapes consisting of two well-defined segments, each of which appears approximately linear on a semilog plot. The initial sharp drop of static stress with

increasing number of pulse cycles is attributed to the transient temperature rise to steady-state conditions. During this period the warming of the wire reduces its tensile strength until the load applied by the dead weight results in an overload condition. After reaching a steady state average temperature the wires are subjected to a combination of cyclic mechanical loading and creep. Under these conditions the wire gradually degrades through accumulated annealing and mechanical damage. In comparing the two curves of Figure 16 it should be remembered that the joule heating input at the 20 amp level is approximately 1.8 times that at the 15 amp condition. Actually, the difference is probably greater due to the increase in resistivity at elevated temperatures.

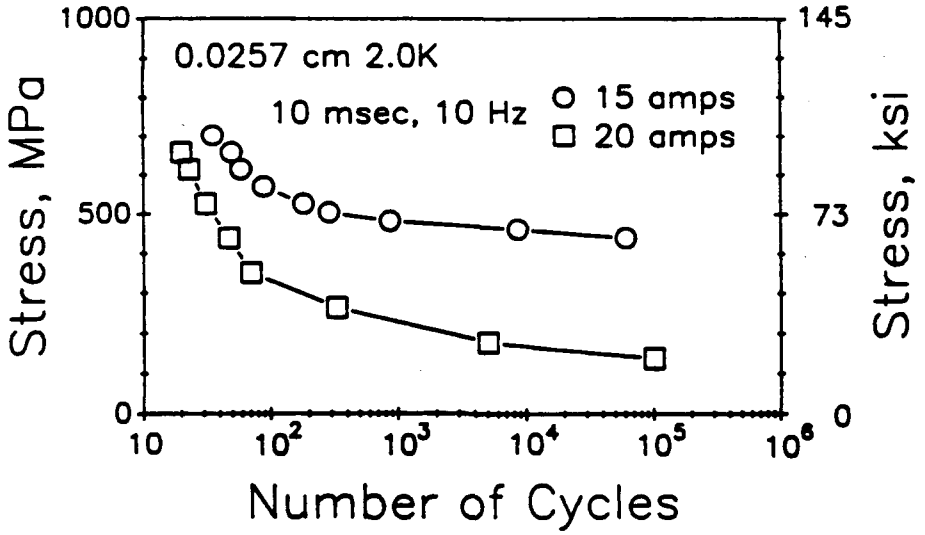

Figure 16. Pulsed current fatigue results of 0.0257 cm 2.0K wires resulting from 10 msec, 10 Hz pulsing at 15 and 20 amps.

The 1.8M composite wires possess outstanding tensile properties as a result of their fine-filament structure. For example, a 0.0267 cm 1.8M wire has a yield strength of 765 MPa (111 ksi) and a tensile strength of 1360 MPa (197 ksi) with a 3.8 percent elongation relative to a 10 cm gage length. The only drawback of fine-filament designs with respect to conductor applications lies in some compromise of electrical properties. The 2.98 μohm-cm electrical resistivity of an as-drawn 0.0267 cm diameter 1.8M wire is 1.2 times that of a 2.0K wire having a similar Nb volume fraction. As such, the application of similar current pulses to the 2.0K and 1.8M wires of the same diameter will cause more heating in the fine-filament composite. In spite of this, the pulsed current fatigue performance of the 1.8M wires is markedly superior to that of the 2.0K wires. As shown in Figure 17, 0.0267 cm diameter 1.8M wires can still support a static stress of 1050 MPa (152 ksi) after ten thousand cycles of 15 amp, 10 msec, 10 Hz pulsed current fatigue. This is more than twice the stress that the 2.0K wires can bear under the same pulse conditions. The superiority of the fine-filament material is even greater under more severe

pulse conditions. The 1.8M wires have a fracture stress of more than 600 MPa (87 ksi) after ten thousand cycles of 20 amp, 10 msec, 10 Hz pulsed current fatigue. The 2.0K data indicates a fracture stress of less than 200 MPa under similar conditions. The much more severe 25 amp, 10 msec, 10 Hz pulse conditions result in 1.8M fracture stresses of less than 300 MPa at long times. The average steady state temperature calculated is apparently too high for sustained high stress operation.

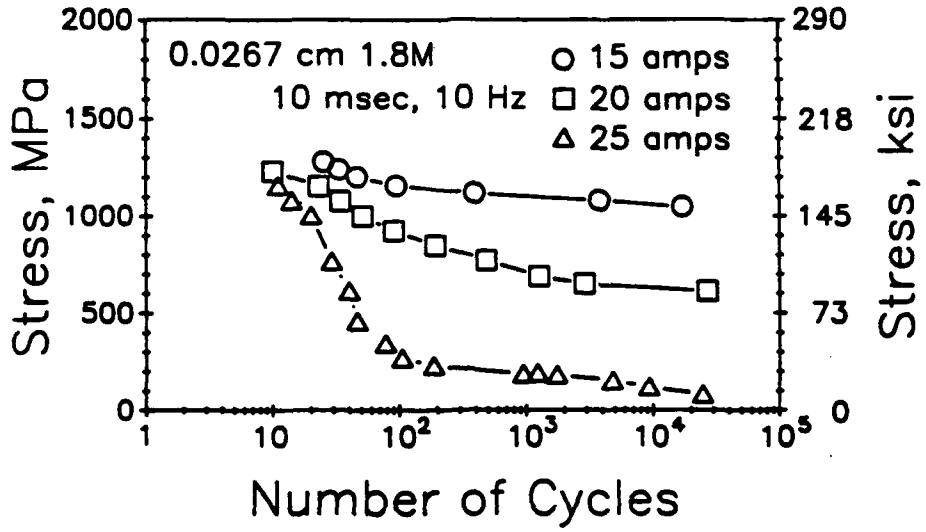

Figure 17. Pulsed current fatigue results of 0.0267 cm 1.8M wires resulting from 10 msec, 10 Hz pulsing at 15, 20, and 25 amps.

5.4.2 Pulse Energy Effects.

The cyclic mechanical loading inherent in pulsed current fatigue arises from the arresting action of the sample wire on the downward motion of the lower grip mass immediately after the end of a pulse. The severity of the post-pulse jerk is governed by the sharpness with which the wires are heated during a pulse. During the application of a direct current pulse the temperature rise and hence the unladen length of the wire will be nearly linear with respect to time. That is, direct current heating tends to extend a conductor at constant velocity. However, the vertical drop of an unsupported lower grip assembly would vary as the square of time under the influence of gravity. A low current pulse results in a low heating rate that allows the descending lower grip assembly to keep up with the extending wire. A long pulse, even one of high current, eventually allows the accelerating lower grip assembly to catch up to the extending wire. Generation of the most severe loading therefore requires rapid heating of the sample wire over a short time interval. Smaller diameter fine-filament wires provide a means of achieving pulsed current fatigue conditions of great mechanical severity at readily attainable current levels.

The selection of the 1.8M composite design for the pulse energy trials was due to the superior performance of the fine-filament composite in the previous section. The mechanical and electrical properties of the 1.8M wires are noticeably dependent upon wire diameter. Smaller wires have reduced interfilament spacings that enhance tensile properties at some expense of electrical conductivity. For example, as-drawn 0.018 cm diameter 1.8M wires have a yield strength of 864 MPa (125 ksi), a tensile strength of 1680 MPa (244 ksi), an elongation of 5.3 % (over a 10 cm gage length), and an electrical resistivity of 3.01 μohm-cm. To demonstrate the influence of mechanical severity on pulsed current fatigue behavior three pulse conditions possessing similar heating characteristics were selected. The average temperature of a wire is primarily dependent on the power that must be dissipated. The average power P_{av} over a pulse cycle is given by

$$P_{av} = \frac{I^2 t}{T} \frac{\rho l}{A}$$

where I is the current during the pulse, t is the duration of the pulse, T is the period of the pulse cycle and ρ, l, and A are the resistivity, length, and cross-sectional area of the wire. Here, it is assumed that the variations of resistivity, length, and area with temperature and loading are represented by appropriate average values. Noting that the period of the pulse cycle T is simply the reciprocal of the pulse frequency, the dependence of the average power on the pulsing conditions becomes

$$P_{av} \alpha I^2 t \nu$$

where ν is the frequency. In comparison, the energy per pulse does not depend on the frequency of pulsing. Once again ignoring variations in length, area, and resistivity, the dependence of pulse energy

$$E \alpha I^2 t$$

is governed by the current and duration of the pulse. The three pulse conditions given in Table 5 were chosen to share the same $I^2 t \nu$ while differing in $E \alpha I^2 t$. Note that the three sets of pulse conditions differ in frequency as well as current and duration. The best comparison between pulsed current conditions of similar average power but different frequency is provided by plotting the experimental static stress values as a function of time rather than number of cycles. As before a logarithmic scale for the abscissa allows all the data to be shown on a single plot. As shown in Figure 18, the differences in pulse energy result in large variations in the ability to bear stress. Under the least severe 10 amps, 10 msec, 13.5 Hz pulse conditions ($I^2 t$ = 1 amp^2-sec) a static stress of 970 MPa can be supported for one thousand seconds. As $I^2 t$ is increased to 6 and 18 amp^2-sec the maximum static stress at a thousand seconds is reduced to 575 MPa and 250 MPa, respectively. Two factors are important in producing

this dramatic sensitivity to pulse energy, maximum stress and peak temperature. The length and stress oscillations shown in Figures 15a and 15b were obtained for the 350 MPa static stress point of the 30 amp, 20 msec, 0.75 Hz (18 amp^2-sec) data. It is interesting to note that the maximum dynamic stress attained under these high pulse energy conditions is less than the static stress that can be supported under the lowest pulse energy conditions. Even though the stress oscillations are quite severe, the peak value of 671 MPa is far below the static stress levels sustainable under the 10 amp, 10 msec, 13.5 Hz pulse conditions. However, although the average wire temperature is nearly the same under the three pulse conditions, the maximum wire temperatures differ greatly.

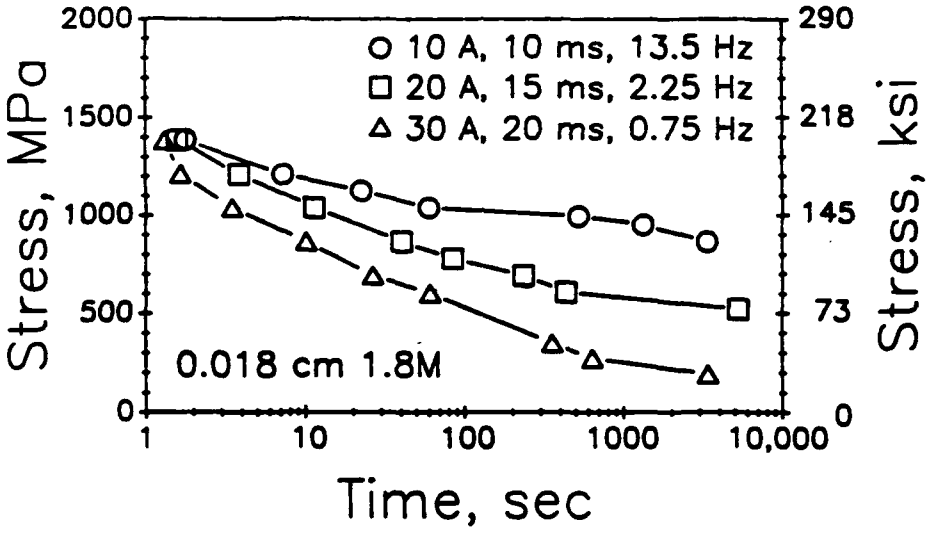

Figure 18. Pulsed current fatigue results of 0.018 cm 1.8M wires resulting from three pulse current fatigue conditions having the same average power input. The lifetime of the conductors is reduced sharply as the pulse energy is increased.

Table 5. Pulsing conditions, I^2tv, and I^2t applied to 0.018 cm diameter 1.8M wires.

current I, (amps)	duration t, (msec)	frequency v, (Hz)	J, (amps/cm^2)	I^2tv, (amp^2)	I^2t, (amp^2-sec)
10	10	13.5	38,900	13.5	1
20	15	2.25	77,700	13.5	6
30	20	0.75	116,000	13.5	18

Fracture surfaces demonstrate the differences in failure mode observed in pulsed current fatigue testing. The initial steeply downward segments of the curves in Figures 16, 17, and 18 are attributed to overload conditions. As the average temperature of a wire approaches a steady-state value its ultimate tensile strength is reduced. When the ultimate tensile strength is reduced to the level of the applied stress, the wire fails. Since all of the wires of this investigation are ductile at room temperature, their failure by tensile overload should produce a ductile fracture. As shown in Figure 19a, the fracture surface obtained under such conditions exhibits a ductile cup-and-cone morphology in which the exterior shear lips surround a dimpled concave interior. This particular fracture was obtained from the initial pulsing of a 0.018 cm diameter 1.8M wire under high current density conditions. The ductility is quite remarkable when the high tensile strength of the conductor is considered. The lower loads required to extend sample life beyond 100 cycles correspond to static stresses considerably less than the tensile strength. As expected, the long-cycle fracture surface shown in Figure 19b indicates failure by a less ductile mechanism. The most obvious difference is the near 45° inclination of the fracture surface to the axis of the wire. This suggests that shear deformation is an important factor in the failure mode. The fracture surface is comprised of three relatively distinct areas; the rim and two interior zones. The perimeter of the 1.8M composite is comprised of a filament-free zone of low strength and poor resistance to annealing. The ductility of the perimeter Cu layer is evidenced by several cracks or tears around the rim. In contrast, the interior filament-laden high strength region exhibits a much less ductile mode of failure. The darkened portion of the interior near the top of the micrograph shows a region that had been exposed before the fracture of the wire. The larger, lighter interior region is characteristic of essentially brittle failure emanating from the previously exposed interior zone. The failure probably started by the exposure of the interior colony structure by shearing of the filament-free outer layer. A gradual progression of the crack into the interior resulted in the darkened region. The resulting overload and stress concentration caused fracture of the remaining cross-section.

5.5 CONCLUSIONS.

A novel test method called pulsed current fatigue was developed to evaluate potential pulsed current conductors. In this technique a periodic pulsed current is applied to a sample conductor wire supporting a dead weight against the acceleration of gravity. The thermal expansion resulting from joule heating of the wire causes cyclic mechanical loading along the axis of the wire. The rapid expansion and contraction caused by the thermal cycling introduce oscillations of the wire-weight spring-mass system. The pulsed current fatigue performance of fine-filament Cu-Nb composites were found to be markedly superior to that of their coarse-filament counterparts. By comparing different pulse conditions having the same average power input, it was shown that a more severe pulse can drastically reduce the load mass that can be supported for a given time.

(a)

(b)

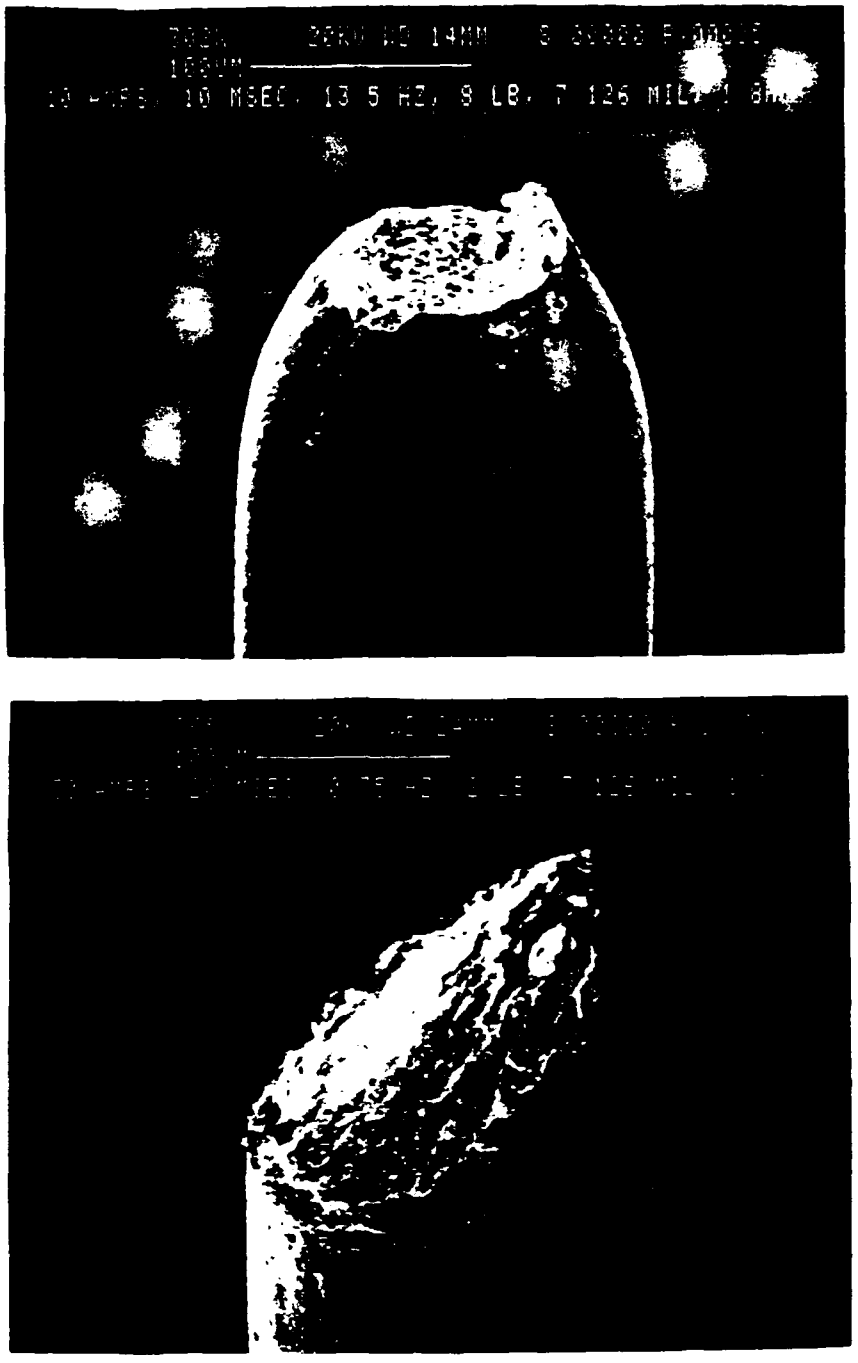

Figure 19. Fracture surfaces of 0.018 cm 1.8M wires subjected to a) 10 amp, 10 msec, 13.5 Hz, 1380 MPa and b) 30 amp, 20 msec, 0.75 Hz, 345 MPa pulsed current fatigue.

SECTION 6

Cu-Ag COMPOSITES

6.1 CONCEPT AND APPROACH.

The multifilamentary composites of this study are intended to obtain the best combination of high mechanical strength and low electrical resistivity. In the case of the Cu-Nb composites of the proceeding sections both the Nb filaments and the Cu matrix contribute to their remarkable mechanical strength. However, because Nb has such a high resistivity only the Cu matrix provides an effective path for electrical conduction. Electrically, the Nb filaments can almost be considered as insulators. The substitution of a high conductivity fiber metal for Nb should significantly enhance the electrical performance of multifilamentary composites.

The choice of an alternative filament material must be made on the basis of mechanical strength, electrical resistivity, and phase diagram limitations. The high mechanical strength of Cu-Nb composites is derived from work hardening of fibers and matrix and the deformation mismatch between Cu and Nb. To retain these strengthening mechanisms the fiber material must be amenable to cold work without annealing and crystallographically dissimilar to the Cu matrix. High electrical conductivity requires the use of a semi-noble or noble metal for the fiber phase. The basic phase diagram limitation is that no brittle phases be formed during billet fabrication. The best compromise between these factors and cost is provided by employing Ag as the fiber phase. Ag has excellent ductility, higher electrical conductivity than Cu, and favorable Cu-Ag phase diagram relationships. The only apparent drawback is the crystallographic similarity to Cu. Since both Cu and Ag are face-centered metals, they differ crystallographically only in lattice parameter. However, Frommeyer and Wassermann (3,4) have fabricated high strength Cu-Ag wires using an *in-situ* process. This section describes the first investigation of continuous-filament Cu-Ag composites.

6.2 SPECIFIC Cu-Ag COMPOSITES.

The microfilamentary Cu-Ag composites of this study were fabricated in-house by EIC Laboratories. Because continuous-filament Cu-Ag composites had not been fabricated previously, an intentionally conservative design was devised. Sub-micron filament diameters were obtained by using a double-extrusion fabrication process. The first-extrusion "1.2K" composite design has 1191 filaments of 4.2 μm nominal diameter at a 0.0254 cm diameter wire size. A cross-section of a 0.195 cm (0.077 inch) diameter coarse-filament 1.2K composite wire is shown in Figure 20a. The thick perimeter can and high 0.32 Ag volume fraction result in some crowding of the filaments in the 1.2K design. The double-extrusion "1.3M" composite design utilizes 1115 colonies of the 1.2K composite to give 1.33 million filaments of 0.11 μm nominal diameter at a

(a)

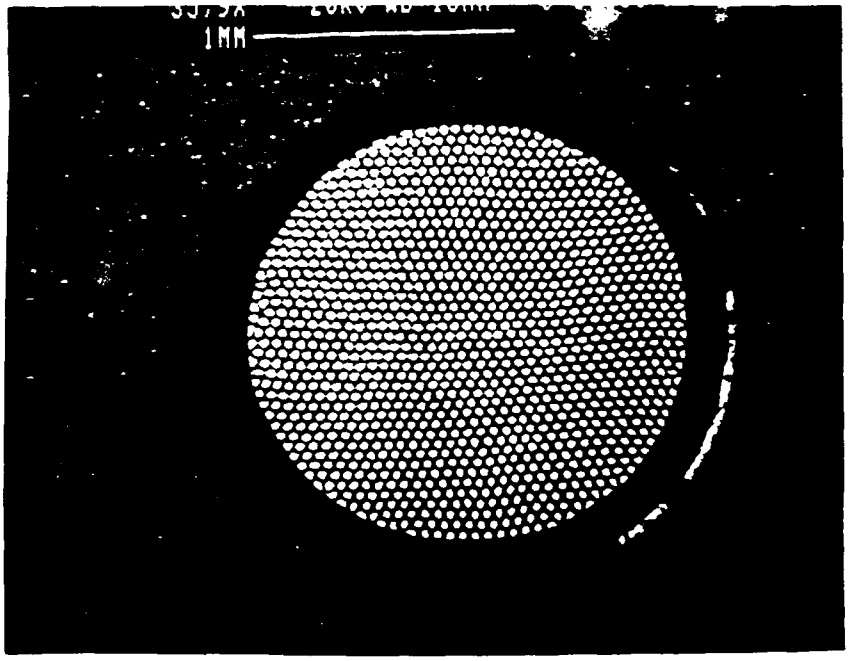

(b)

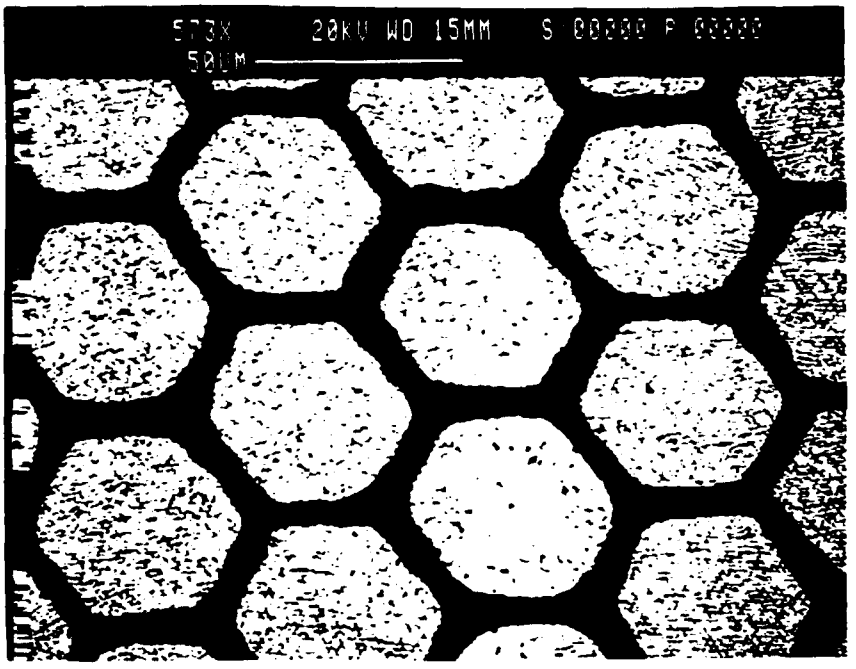

Figure 20. Cross-sections of (a) the 1.2K coarse-filament and (b) the 1.3M fine-filament Cu-Ag composites of this study. The 1.2K wire is derived from a single-extrusion billet whereas the 1.3M material is the result of a double-extrusion fabrication.

0.0254 cm wire diameter. A scanning electron micrograph of a portion of the cross section of a 0.073 cm (0.029 inch) fine-filament 1.3M composite wire is shown in Figure 20b. Because of the conservative design of the 1.2K composite wire feedstock used to stack the 1.3M billet there is a thick filament-free Cu region between the colonies. This necessarily results in some compromise of strength because a significant portion of the Cu matrix does not benefit from the presence of the reinforcing filaments. Special efforts, such as centerless grinding of the first extrusion and use of a thinner perimeter can, would allow a more uniform filament distribution.

Both of the Cu-Ag composites of this study are continuous filament designs. Each filament extends throughout the length of the wire, whether the length be 1 cm or several kilometers. A significant benefit of the continuous design is an extraordinary uniformity of properties both along each wire's length and between wires of identical specification. Each filament of a given design has received the same deformation and should have uniform properties. However, there are three distinct Cu regions in the 1.3M composite that are expected to have different physical characteristics. Because the interfilament Cu is finely partitioned by the Ag fibers, it receives severe mechanical deformation during wire drawing to final size. This allows the strength of the interfilament Cu to increase rapidly as the deformation proceeds. Since the filament-free Cu between the colonies and in the perimeter can of the 1.3M composite is less severely constrained, it will exhibit lower mechanical strength. The specifications of the composites are summarized in Table 6.

Table 6. Design parameters for the 1.2K and 1.3M Cu-Ag composite wires.

Composite Designation	1.2K	1.3M
Number of Colonies	1	1115
Filaments per Colony	1191	1191
Total Number of Filaments	1191	1.33×10^6
Overall Ag Volume Fraction	0.32	0.23
Local Nb Volume Fraction	0.44	0.44
Nominal Fiber Diameter at 0.0254 cm wire size	4.2 μm	0.11 μm

6.3 RESULTS AND DISCUSSION.

Since the 1.3M Cu-Ag composite is intended to be an improvement over the fine-filament Cu-Nb designs, it is natural to compare its mechanical and electrical properties to those of the 1.8M and 2.2M wires. The ultimate tensile strength of the 1.3M Cu-Ag, 1.8M Cu-Nb, and 2.2M Cu-Nb composites are shown as a function of root reciprocal wire diameter in Figure 21. At all wire

sizes the Cu-Ag composite is weaker than its Cu-Nb counterparts. This is a result of three factors. Since Ag is inherently weaker than Nb, the initial strength of the Cu-Ag composite is less than that of the Cu-Nb wires. Additionally, the uneven filament distribution across the Cu-Ag composite leaves a substantial portion of the cross-section unreinforced. The lower slope of the Cu-Ag curve of Figure 21 indicates that the crystallographic similarity of Ag and Cu provides a strengthening mechanism that is less rapid than that inherent in Cu-Nb wires.

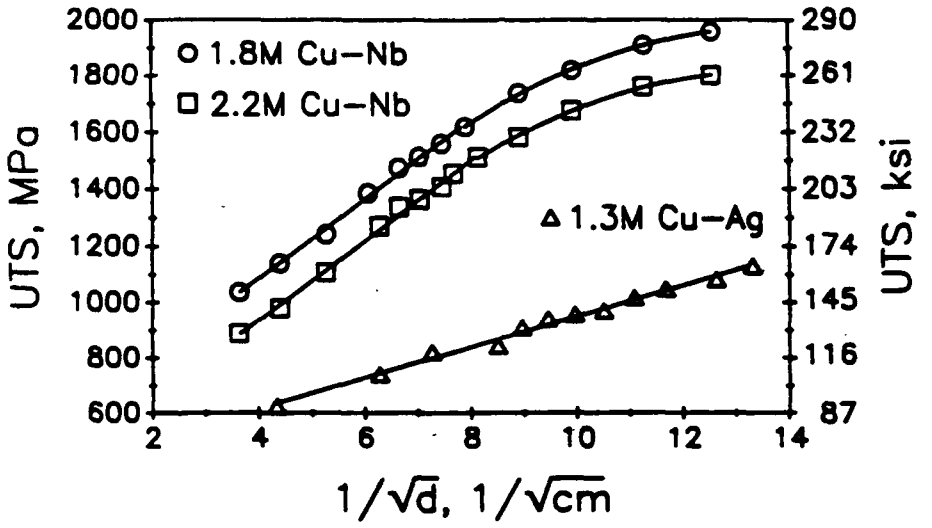

Figure 21. Ultimate tensile strength as a function of root reciprocal wire size for the fine filament 1.3M Cu-Ag, 1.8M Cu-Nb, and 2.2M Cu-Nb composite wires.

The Cu-Ag composite was fabricated to benefit from the high electrical conductivity of Ag. Since the resistivity of Ag is actually less than that of Cu, the Cu-Ag wires should enjoy an appreciable resistivity advantage over the Cu-Nb samples. The resistivity of each of the three composites as a function of reciprocal wire size is shown in Figure 22. For all wire sizes investigated, the resistivity of the 1.3M Cu-Ag composite is less than those of the Cu-Nb composites. Moreover, the linearity of the Cu-Ag ρ *vs.* $1/d$ plot prevails over the entire size range investigated. At the largest wire sizes the resistivity benefits are essentially those expected by the replacement of the resistive Nb with conductive Ag. That is, the large diameter 2.2M wires are approximately 20% and the 1.8M wire are more than 30% more resistive than the Cu-Ag wires. At the smaller wire sizes (higher $1/d$ values) the disparity is even more pronounced. This implies that the dislocation density increases less rapidly in the Cu-Ag composites than in the Cu-Nb wires. Nb seems to be a significantly more aggressive reinforcing phase than is Ag. This is not unexpected given the similarity of the Cu and Ag face-centered lattices. However, the fact that the linear-

ity of the Cu-Ag plot extends to the finest wire sizes suggests that the 1.3M composite could be drawn to finer interfilament spacings than were possible with the Cu-Nb wires.

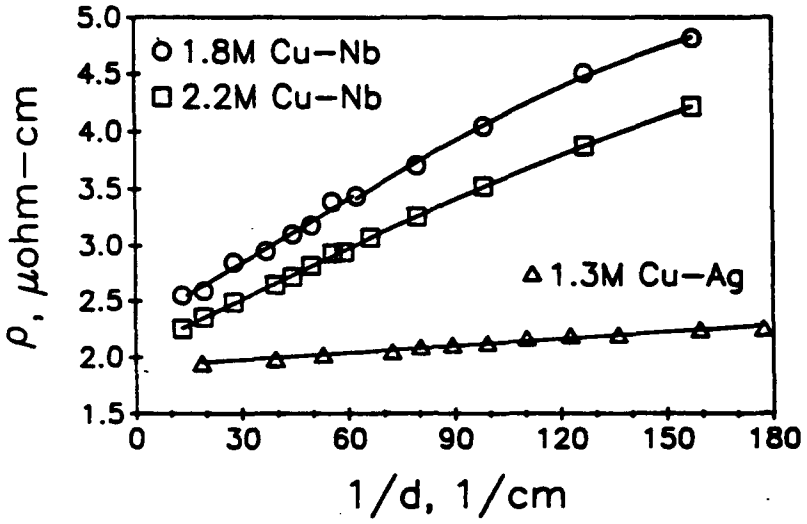

Figure 22. Electrical resistivity as a function of reciprocal wire size for the fine filament 1.3M Cu-Ag, 1.8M Cu-Nb, and 2.2M Cu-Nb composite wires.

The deformation inherent in room temperature wire drawing introduces a large degree of cold work in the composite wires. The major influence of this deformation on the microstructure is to increase dramatically the density of defects. The defects, predominantly crystal lattice distortions called dislocations, act to hinder further deformation of the materials. Heavily deformed materials such as small wires tend to be strong by virtue of a their high dislocation densities. In the present case of fine-filament composites both the filaments and the matrix are known to experience dramatic rises in dislocation density as the wires are deformed during drawing. The distortion of the microstructure inherent in dislocations acts to disrupt electrical conduction. An indication of the dislocation density in the Cu can be gained by considering the electrical resistivity of the wires. The lower slope of the Cu-Ag line in Figure 22 can only partially be explained by the higher electrical conductivity of the Ag. This indicates that the closer match in matrix-filament deformation inherent in the Cu-Ag system produces a lower work hardening rate than that which prevails in the case of Cu-Nb. This does not mean that high strengths cannot be attained in the Cu-Ag system. It does imply that more deformation and finer filament sizes are required to access the highest strength levels.

The fine-filament 1.2K data is fitted by a single straight line indicating that electrical resistivity is given by

$$\rho = \rho_o + \frac{k}{d} .$$

The experimental results of Rider and Foxon (12) and the theoretical considerations of Brown (13) suggest that Cu resistivity is directly proportional to dislocation density with a Cu dislocation resistivity on the order of 2×10^{-19} Ωcm^3. Therefore the dislocation density in the Cu-Ag curve of Figure 22 curve is given by

$$\rho_{dis} \alpha \frac{k'}{d} .$$

Noting that the dependence of strength on dislocation density is given by $\sigma = \sigma_o + k\sqrt{\rho_{dis}}$ (14), the dependence of strength on wire size becomes

$$\sigma = \sigma_o + \frac{k}{\sqrt{d}}$$

which is the Hall-Petch relationship. Thus the strengthening behavior noted in the Cu-Ag composites of this study is consistent with both the spacing of barriers (the Cu matrix-Ag filament interfaces) and the increase in dislocation density (form wire drawing deformation).

From an applications viewpoint, it is the tradeoff between strength and electrical conductivity that is most important. It is important to determine whether fine-filament Cu-Ag composites provide a better tradeoff than their Cu-Nb counterparts. This is addressed by Figure 23 in which the electrical conductivities of the three fine-filament composites are plotted as a function of ultimate tensile strengths. For each composite conductivity is linear with respect to ultimate tensile strength. However, the 1.3M Cu-Ag line clearly lies above the single line fitting the 1.8M and 2.2M Cu-Nb data. Thus, the Ag filaments do provide a better conductivity-strength combination. The extrapolation of the Cu-Ag data to higher strength levels indicates that the advantage should increase as the strength increases.

6.4 CONCLUSION.

The strengthening of fine-filament Cu-Ag composites with decreasing wire size is described by a Hall-Petch (10,11) relationship $\sigma = \sigma_o + k/\sqrt{d}$. It is likely that the strengthening occurs through a combination of interface barriers and dislocation density. The resistivity of wire of different sizes is closely described by $\rho = \rho_o + k/d$. In considering the tradeoff between electrical conductivity and mechanical strength, the fine-filament Cu-Ag wires are clearly superior to their Cu-Nb counterparts. However, the strengthening provided by the Ag filaments is apparently not as rapid as that observed in Cu-Nb composites. Although the conservative 1.3M design did not provide access to the highest strength levels, the path to higher Cu-Ag strength is evident. By incorporating some relatively

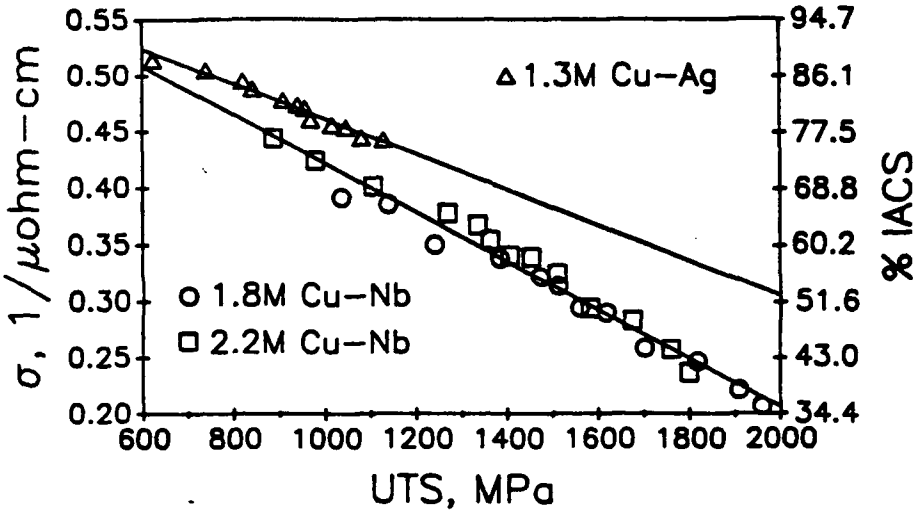

Figure 23. Electrical conductivity as a function of ultimate tensile strength for the fine-filament 1.3M Cu-Ag, 1.8M Cu-Nb, and 2.2M Cu-Nb composite wires.

straightforward steps in the fabrication process the distribution of filaments can be made much more uniform. This will extend the fine-filament strengthening mechanism to the entire composite cross-section. Additionally, the utilization of finer sized Ag in the initial billet will allow finer interfilament spacings to be accessed at larger composite diameters. The fact that the Cu-Ag strength and resistivity curves show no tendency to saturate indicates that more strengthening would be available in a second-generation composite.

SECTION 7

RECOMMENDATIONS

The mechanical and electrical properties of continuous-filament Cu-Nb and Cu-Ag composites have been surveyed. The microfilamentary Cu-Nb composites were found to have excellent mechanical strength, good electrical conductivity, substantial resistance to annealing, and remarkable pulsed current fatigue capabilities. As such, the fine-filament Cu-Nb composites should be considered as an excellent material for high strength electrical conductors. They could be employed in wire, rod, or plate form. Consideration of continuous-filament Cu-Nb composites as monolithic load-bearing members would necessitate the characterization of a large-scale composite in which fine filament sizes were available in rod or plate rather than wire form. Naturally, a more complete characterization of electrical and mechanical properties would be required for specific applications. For example, the transverse properties of these materials have not yet been determined.

The Cu-Ag composites present an interesting alternative to the Cu-Nb system. The anticipated electrical conductivity advantage afforded by Ag filaments was confirmed. Indeed, extrapolation of their conductivity vs. strength behavior indicates that the advantage of Cu-Ag over Cu-Nb will increase at the higher strength levels. However, since Ag is not as aggressive as Nb with regard to developing strength by cold work, the strengths of the present Cu-Ag wires do not approach those of the best Cu-Nb samples. Although the present data suggests that higher strength levels can be accessed, a second-generation Cu-Ag composite program would be required for demonstration.

SECTION 8

LIST OF REFERENCES

1. H.E. Cline, B. Strauss, R.M. Rose, and J. Wulff, Trans. Q. 59, 132 (1966).
2. D.L. McDanels, R.W. Jech, and J.W. Weeton, Trans. AIME 233, 636 (1965).
3. G. Frommeyer and G. Wassermann, Acta Metall. 23, 1353 (1975).
4. G. Frommeyer and G. Wassermann, Phys. Status Solidi 27, 99 (1975).
5. J. Bevk, J.P. Harbison, and J.L. Bell, J. Appl. Phys. 49, 6031 (1978).
6. K.R. Karasek and J. Bevk, J. Appl. Phys. 52, 1370 (1981).
7. D.E. Cohen and J. Bevk, Appl. Phys. Lett. 39, 595 (1981).
8. W.F. Hosford, Trans. AIME 230, 12 (1964).
9. J.D. Klein and R.M. Rose J. Appl. Phys. 61, 2212 (1987).
10. E.O. Hall, Proc.Phys. Soc. B 64, 747 (1951).
11. N.J. Petch, J. Iron Steel Inst. 174, 25 (1953).
12. J.G. Rider and C.T.B. Foxon, Philos. Mag. 16, 1133 (1967).
13. R.A. Brown, J. Phys. F 7, 1283 (1977).
14. K.M. Ralls, T.H. Courtney, and J. Wulff, *Introduction to Materials Science and Engineering* (John Wiley & Sons, New York, 1976), p. 450.
15. J.D. Verhoeven, H.L. Downing, L.S. Chumbley, and E.D. Gibson, J. Appl. Phys. 65, 1293 (1989).
16. J.W. Ekin, Adv. in Cryo. Eng. 24, 306 (1978).
17. C.C. Koch and D.S. Easton, Cryogenics 17, 391 (1977).
18. W. Schlump, H. Freyhart, and E. Nembach, Acta. Met. 20, 257 (1972).
19. R. Bormann, J. Appl. Phys. 54, 1479 (1983).
20. J.D. Verhoeven, E.D. Gibson, F.C. Laabs, J.E. Ostenson, and D.K. Finnemore, IEEE Trans. Mag. MAG-19, 563 (1983).
21. A.T. Santhanam, J. Mat. Sci. 11, 1099 (1976).
22. E.J. Kramer, J. Appl. Phys. 44, 1360 (1973).
23. M.P. Mathur, M. Askin, and D.W. Deis, J. Appl. Phys. 45, 3627 (1974).
24. H.E. Cline, B.P. Strauss, R.M. Rose, and J. Wulff, J. Appl. Phys. 37, 5 (1966).
25. H.E. Cline, B. Strauss, R.M. Rose, and J. Wulff, Transactions Quarterly 59, 132 (1966).

26. J.D. Klein, Sc.D. Thesis, Department of Materials Science and Engineering, M.I.T., Cambridge, MA (1984).

27. E.J. Kramer, J. Electron. Mater. 4, 839 (1975).

28. J.E. Evetts and C.J.G. Plummer in *Proceedings of International Symposium on Flux Pinning and Electromagnetic Properties in Superconductors*, ed. T. Matsushita, K. Yamafuji, and F. Irie (Matsukuma Press, Fukuoka), p. 146.

29. J.D. Klein and R.M. Rose, J. Appl. Phys. 61, 2979 (1987).

30. D.C. Hill and R.M. Rose, Met. Trans. 2, 1433 (1971).

31. Innovative Science and Technology Office bulletin on the Technical Program Information of the Strategic Defense Initiative Organization (1988).

32. J.D. Klein and R.M. Rose, J. Appl. Phys. 67, 930 (1990).

APPENDIX A

PERSONNEL

Several staff and senior personnel aided in the completion of this research project. The experimental laboratory work was performed by Mr. Allen Yen and Mr. Louis L. Wu. Experimental design, composite design, and technical reporting were undertaken by Dr. James D. Klein. Dr. Stuart F. Cogan was responsible for overall program management.

The resumes of Drs. James D. Klein and Stuart F. Cogan follow.

DR. JAMES D. KLEIN
Senior Materials Scientist
EIC Laboratories, Inc.

Education:

B.S.E. Mechanical Engineering, Duke University, 1974.
M.S. Materials Science, Duke University, 1976.
Sc.D. Materials Science, Massachusetts Institute of Technology, 1984.

Professional Experience:

1987-Present	Senior Scientist in Materials Research, EIC Laboratories, Inc.
1984-1987	Assistant Professor, Department of Metallurgical Engineering, Michigan Technological University.
1979-1984	Research Assistant, Department of Materials Science and Engineering, Massachusetts Institute of Technology.
1978-1979	Process Engineer; POY Process Group, FII Research and Development, Fiber Industries Inc.
1977-1978	Research Associate; Department of Mechanical Engineering and Materials Science, Duke University.
1976-1977	Process Engineer; Process Engineering Group, Research Triangle Institute.

Honors

1973	Pi Tau Sigma, Tau Beta Pi, Duke University, Durham, NC
1974	Phi Beta Kappa, summa cum laude, Duke University, Durham, NC

Publications:

S. F. Cogan, F. W. Gayle, J. D. Klein, F. H. Cocks, and M.L. Shepard; "Extraction and X-ray Analysis of Phases in Aluminum Alloys", J. Mater. Sci. 13, 2687 (1978).

S. F. Cogan, D. S. Holmes, J. D. Klein, and R. M. Rose; "Multifilamentary Nb_3Sn by an Improved External Diffusion Method", Filamentary A15 Superconductors, ed. M. Suenaga and A. F. Clark, Plenum Press, New York 91 (1980).

J. D. Klein, S. F. Cogan, G. Warshaw, N. Dudziak, and R. M. Rose; "Properties of Microfilamentary Superconducting Composites Produced by a Modified External Diffusion Method", IEEE Trans. Mag. MAG-17, 378 (1981).

J. D. Klein, G. Warshaw, N. Dudziak, S. F. Cogan, and R. M. Rose; "On the Suppression of Kirkendall Porosity in Multifilamentary Superconducting Composites", IEEE Trans. Mag. MAG-17, 380 (1981).

J. D. Klein, S. F. Cogan, S. Kwon, and R. M. Rose; "Manufacture of Multifilamentary Nb_3Sn Superconductors by the External Diffusion Method: Tin Coalescence and Diffusion", 9th Symposium on Engineering Problems of Fusion Research, ed. C.K. Choi, IEEE, New York 1310 (1981).

S. Kwon, S. F. Cogan, J. D. Klein, and R. M. Rose; "The Influence of Gallium on External Diffusion Processed Nb_3Sn Composites", J. Appl. Phys. 54, 1008 (1983).

S. F. Cogan, J. D. Klein, S. Kwon, H. Landis, and R. M. Rose; "On the Mechanical Properties of Sn-Core Processed Nb_3Sn Filamentary Composites", IEEE Trans. Mag. MAG-19, 917 (1983).

S. F. Cogan, S. Kwon, J. D. Klein, and R. M. Rose; "Fabrication of Large Diameter External Diffusion Processed Nb_3Sn Composites", IEEE Trans. Mag. MAG-19, 1139 (1983).

S. F. Cogan, S. Kwon, J. D. Klein, R. M. Rose; "Diffusion in the CuSn Binary System: Application to Nb_3Sn Composites", J. Mat. Sci. 19, 497 (1984).

J. D. Klein and R. M. Rose; "Thermal Behavior and Strength of Continuous Filament Cu-Nb Composites", J. Appl. Phys. 58, 2212 (1987).

J. D. Klein and R. M. Rose; "The Effect of Strain on the Critical Current Density of Cu-Nb Composites", J. Appl. Phys. 61, 2979 (1987).

J. D. Klein, S. L. Clauson, and S. F. Cogan; "Morphology and Charge Capacity of Sputtered Iridium Oxide Films", J. Vac. Sci. Technol. A 7, 3043 (1989).

J. D. Klein, S. L. Clauson, and S. F. Cogan; "The Influence of Substrate Bias on the Morphology and Charge Capacity of rf Sputtered Iridium Oxide Films", J. Mater. Res. 4, 1505 (1989).

J. D. Klein and A. Yen; "Optical Plasma Monitoring of Y-Ba-Cu-O rf Sputter Target Transients", Appl. Phys. Lett. 55, 2670 (1989).

J. D. Klein and A. Yen; "The Influence of Radio Frequency Sputter Variables on the Composition of $YBa_2Cu_3O_7$ Films", J. Vac. Sci. Technol. A 8, 1 (1990).

J. D. Klein and R. M. Rose; "The Effect of Heat Treatment on the Superconducting Properties of Cu-Nb Composites", J. Appl. Phys. 67, 930 (1990).

J. D. Klein, A. Yen, and S. L. Clauson; "Ion Beam Deposition of *In-Situ* Superconducting Y-Ba-Cu-O Films", Appl. Phys. Lett. 56, 394 (1990).

J. D. Klein, A. Yen, and S. L. Clauson; "Ion Beam Sputtering of *In-Situ* Superconducting Y-Ba-Cu-O Films", J. Appl. Phys. 67, 6389 (1990).

J. D. Klein, A. Yen, and S. F. Cogan; "Determining Thin Film Properties by Fitting Optical Transmittance", accepted for August J. Appl. Phys. (1990).

J.D. Klein and A. Yen; "Optical Plasma Monitoring of Y-Ba-Cu-O Sputter Target Transients", Proceedings Spring 1990 MRS Meeting M6.10, San Francisco, CA (1990).

J. D. Klein and A. Yen; "Optical Monitoring of Ion Beam Y-Ba-Cu-O Sputtering", accepted for November J. Appl. Phys. (1990).

DR. STUART F. COGAN
Head of Materials Science
EIC Laboratories, Inc.

Education:

Sc.D., Materials Science, Massachusetts Institute of Technology, 1979.
M.S., Materials Science, Duke University, 1977.
B.S., Mechanical Engineering, Duke University, 1975.

Professional Experience:

1986 - Present	Head of Materials Science, EIC Laboratories, Inc.
1983 - 1986	Senior Scientist, EIC Laboratories, Inc.
1980 - 1983	Research Associate, Department of Materials Science and Engineering, Massachusetts Institute of Technology.
1979 - 1980	Visiting Assistant Professor, Department of Mechanical Engineering and Materials Science, Duke University.

Publications:

S.F. Cogan and F.H. Cocks, "A Method for Mounting Powder Samples that Avoids Adverse Strain Effects at Low Temperatures," J. Appl. Cryst. **8**, 571 (1975).

F.H. Cocks and S.F. Cogan, "A New Source of X-ray Line Broadening: Inhomogeneous Strains Induced by Uniform Homogeneous Temperature Conditions in Polyphase or Non-cubic Materials," J. Mat. Sci. **11**, 2061 (1976).

S.F. Cogan, J.E. Rockwell III, F.H. Cocks, and M.L. Shepard, "Preparation of Metallic and Intermetallic Powders by Spark Erosion," J. Phys. E: Sci. Instrum. **11**, 1974 (1978).

S.F. Cogan, F.W. Gayle, J.D. Klein, F.H. Cocks, and M.L. Shepard, "Extraction and X-ray Analysis of Phases in Aluminum Alloys," J. Mat. Sci. **13**, 2687 (1978).

S.F. Cogan, D.S. Holmes, and R.M. Rose, "On the Micromechanics of Multifilamentary Superconducting Composites," IEEE Trans. on Magn. **MAG-15**, 684 (1979).

S.F. Cogan and R.M. Rose, "On the Elimination of Kirkendall Voids in Superconducting Composites," Appl. Phys. Lett. **35**, 557-559 (1979).

S.F. Cogan and R.M. Rose, "Fatigue Effects in Unidirectional Composites: Applications of Nb_3Sn Superconductors," Appl. Phys. Lett. **35**(11), 884-886 (1979).

S.F. Cogan and R.M. Rose, "Properties of CuSn Bronze at 4.2 K," Cryogenics, pp. 303-316 (June 1980).

S.F. Cogan and R.M. Rose, "Crystallographic Texturing in Nb_3Sn Multifilamentary Superconducting Composites," J. Appl. Phys. **51**(3), 1711-1713 (1980).

S.F. Cogan, D.S. Holmes and R.M. Rose, "Microfilamentary Superconducting Composites by the External Diffusion Method: Nb_3Sn," J. Appl. Phys. **51**(8), 4332-4337 (1980).

S.F. Cogan, J.D. Klein, D.S. Holmes and R.M. Rose, "Microfilamentary Superconductors for Fusion Energy Applications," 8th International Conference on Plasma Physics and Controlled Nuclear Fusion Research, July 1980.

F.H. Cocks, A. Scharman, P.L. Jones and S.F. Cogan, "Hydrogenated A-Si Thin Films Produced by Ion-Plating," Appl. Phys. Lett., **36**(11), 909-910 (1980).

S.F. Cogan, D.S. Holmes, J.D. Klein and R.M. Rose, "Multifilamentary Nb_3Sn by an Improved External Diffusion Method," in Filamentary A15 Superconductors, eds. M. Suenaga and A. T. Clark, Plenum Press, New York p. 91 (1980).

J.D. Klein, S.F. Cogan, G. Warshaw, N. Dudziak and R.M. Rose "Properties of Microfilamentary Superconducting Composites Produced by a Modified External Diffusion Method," IEEE Trans. on Magn. **MAG-17**, 378 (1981).

J.D. Klein, S.F. Cogan, G. Warshaw, N. Dudziak and R.M. Rose, "On the Suppression of Kirkendall Porosity in Multifilamentary Composites," IEEE Trans. on Magn. **MAG-17**, 380 (1981).

J.D. Klein, S.F. Cogan, S. Kwon and R.M. Rose, "Manufacture of Multifilamentary Nb_3Sn Superconductors by the External Diffusion Method: Tin Coalescence and Diffusion," 9th Symposium on Engineering Problems of Fusion Research, ed. C.K. Choi, IEEE, New York 1310 (1981).

S.F. Cogan, J.D. Klein, S. Kwon and R.M. Rose, "Fabrication of Large Diameter External Diffusion Processed Nb_3Sn Composites," IEEE Trans. on Magn. **MAG-19** 917 (1983).

S.F. Cogan, J.D. Klein, S. Kwon, H. Landis and R.M. Rose, "On the Mechanical Properties of Sn-Core Processed Nb_3Sn Filamentary Composites," IEEE Trans. on Magn. **MAG-19**, 917 (1983)

R. Schwall, G. Ozeryansky, S.F. Cogan and R.M. Rose, "Properties and Performance of High Current Density Sn-Core Processed MF Nb_3Sn," IEEE Trans. on Magn. **MAG-19**, 454 (1983).

S. Kwon, S.F. Cogan, J.D. Klein and R.M. Rose, "The Influence of Gallium on External Diffusion-Processed Nb_3Sn Composites," J. Appl. Phys., **54**(2), 1008-1012 (1983).

S.F. Cogan, S. Kwon, J.D. Klein and R.M. Rose "Diffusion in the CuSn Binary System: Application to Nb_3Sn Composites," J. Mat. Sci., **19**, 497-500 (1984).

R.D. Rauh, S.F. Cogan and M.A. Parker, "Materials for Electrochromic Windows," SPIE Vol. **502**, 38-45 (1984).

R.D. Rauh, S.F. Cogan and M.A. Parker, "Infrared Reflectivity Modulation in Li Inserted Electrochromic WO_3 Films," Fall Meeting of The Electrochemical Society, New Orleans, October 7-14, 1984.

S.F. Cogan, E.J. Anderson, T.D. Plante and R.D. Rauh, "Electrochemical Investigation of Electrochromism in Transparent Conductive Oxides," Applied Optics, **24**(15), 2282 (1985).

S.F. Cogan, E.J. Anderson, T.D. Plante and R.D. Rauh, "Materials and Devices in Electrochromic Window Development," SPIE Vol. **562**, 23-31 (1985).

S.F. Cogan, T.D. Plante, M.A. Parker and R.D. Rauh, "Free-electron Electrochromic Modulation in Crystalline Li_xWO_3," J. Appl. Phys., **60**(8), 2735 (1986).

S.F. Cogan, T.D. Plante, M.A. Parker and R.D. Rauh, "Electrochromic Solar Attenuation in Crystalline and Amorphous Li_xWO_3," Solar Energy Materials, **14**, 185 (1986).

S.F. Cogan, T.D. Plante, R.S. McFadden and R.D. Rauh, "Optical Switching in 'Complementary' Electrochromic Windows," SPIE Vol. **692**, 32-38 (1986).

S.F. Cogan, T.D. Plante, R.S. McFadden and R.D. Rauh, "Solar Modulation in a-WO_3/a-IrO_2 and c-$K_xWO_{3+(x/2)}$/a-IrO_2 Complementary Electrochromic Windows", Solar Energy Materials, **16**, 371-382 (1987).

S. F. Cogan, T.D. Plante, R.S. McFadden and R.D. Rauh, "Design and Optical Modulation of a-WO_3/a-IrO_2 Electrochromic Windows, Proc. SPIE, **823**, 106-112 (1987).

L.S. Robblee and S.F. Cogan, "Metals for Medical Electrodes," Encyclopedia of Materials Science & Engineering, Supplementary Volume 1, ed. Robert W. Cahn, Pergamon Press, Oxford, U.K. pp. 276-281, 1988

R.D. Rauh and S.F. Cogan, "Counter Electrodes in Transmissive Electrochromic Light Modulators," Solid State Ionics, Vols **28-30** Part 2 pp 1707-1714 (1988).

S.F. Cogan, N.M. Nguyen, S.J. Perrotti and R.D. Rauh, "Electrochromism in Sputtered Vanadium Pentoxide," Proc. SPIE, 1989, **1016** 57 (1989)

S.F. Cogan, N.M. Nguyen, S.J. Perrotti, and R. David Rauh, "Optical Properties of Electrochromic Vanadium Pentoxide," J. Appl. Phys. **66**,1333 (1989).

S.F. Cogan, R.D. Rauh, J.D. Westwood, D.I. Plotkin and R.B. Jones, "Infrared Properties of Electrochromic Materials," Proc. SPIE, 1149, 2 (1989).

S.F. Cogan, "Electrochromic Vanadium Pentoxide," in Large Area Chromogenics, edited by C. Lampert and C. Granqvist, SPIE 1990, in press

S.F. Cogan and R.D. Rauh, "The a-WO_3/a-IrO_2 Electrochromic System," in Large Area Chromogenics, edited by C. Lampert and C. Granqvist, SPIE 1990, in press

J.D. Klein, S.L. Clauson, and S.F. Cogan, "Morphology and Charge Capacity of Sputtered Iridium Oxide Films," J. Vac. Sci. Technol. A7, 3043 (1989)

J.D. Klein, S.L. Clauson, and S.F. Cogan, "The Influence of Substrate Bias on the Morphology and Charge Capacity of RF-sputtered Iridium Oxide Films," J. Mater. Res., 4, 1505 (1989)

APPENDIX B

PUBLICATION

One publication resulting from this research project has already appeared: "The Effect of Heat Treatment on the Superconducting Properties of Cu-Nb Composites" by J.D. Klein and R.M. Rose, J. Appl. Phys. 67, 930 (1990).

A copy of this paper follows.

The effect of heat treatment on the superconducting properties of Cu-Nb composites

J. D. Klein
EIC Laboratories, Inc., Norwood, Massachusetts 02062

R. M. Rose
Department of Materials Science and Engineering, Massachusetts Institute of Technology, Cambridge, Massachusetts 02139

(Received 31 July 1989; accepted for publication 28 September 1989)

Microfilamentary composites of continuous Nb fibers in Cu matrices were tested for superconducting transport properties after heat treatments at 200–900 °C. The critical current density at applied magnetic field was reduced dramatically as the heat treatment temperature was increased. The scaling relations describing the critical current as a function of applied field shifted from conventional $(1-h)^2$ scaling to higher-order relations as the heat treatment history was varied. Critical temperature transitions were abnormally broad in the fine-filament composites examined. The upper critical fields and transition temperatures approached bulk values after severe heat treatment.

I. INTRODUCTION

The effect of heat treatment on the nonsuperconducting electrical properties of multifilamentary Cu-Nb composites has been addressed by several investigations.[1-3] Since the normal-state conductivity of Cu is so much greater than that of Nb, these studies have served largely to indicate the annealing and interfacial scattering behavior of the Cu matrix as constrained by the Nb filaments. Resistivity studies of *in situ* composites as a function of temperature have been pursued to indicate the annealing behavior of the Cu.[1,2] Resistivity and thermal contraction observations of continuous filament Cu-Nb composites have related matrix annealing behavior to the relief of large residual strains introduced during cold drawing to final wire size.[3] However, heat treatment at even moderate temperatures can be expected to alter the properties of the small Nb filaments as well as the surrounding Cu matrix. The effects of heat treatment on the Cu and Nb can be partially separated by considering the superconducting behavior of the composites. Since the Cu matrix is not superconducting, the critical current and transition temperature of the composites are governed by the properties of the Nb filaments. The present work on continuous-filament materials produced by stack-and-draw methods describes superconducting behavior in multifilamentary Cu-Nb composites in which there is little chance of filament contamination by matrix Cu during fabrication.

The heat treatment of Cu-Nb composite wires might change the superconducting properties by altering either the Cu matrix or the Nb filaments. Superconducting wires comprised of multifilamentary Nb_3Sn in a bronze matrix respond strongly to their residual stress states at 4.2 K.[4,5] Recent experiments show that annealing cold-drawn Cu-Nb composite wires at temperatures as low as 300 °C can strongly alter the residual stresses present at room temperature.[3] Additionally, the residual stress state of the Nb filaments at 4.2 K will be influenced by the differing thermal contractions of Cu and Nb as well as the possible complication of plastic deformation in an annealed Cu matrix. The effect of heat treatment temperatures up to 900 °C on the internal structure of Nb filaments is not well defined. Moderately deformed Nb single crystals have exhibited no thermally activated dislocation motion below 1000 °C.[6] Although 900 °C is less than half the absolute melting point of Nb, the coalescence observed in fine-filament Cu-Nb composites[7,8] indicates that major changes can occur within the Nb fibers at much lower temperatures.

The critical current density J_c at an applied magnetic field H may be enhanced or degraded as the filament size is decreased. At filament diameters greater than 1 μm, it is generally observed that increasing cold work enhances the J_c of Nb.[9] Indeed, this trend as well as an adherence to Kramer[10] scaling was indicated in the magnetization experiments of Mathur, Ashkin, and Deis[11] for Cu-Nb composites having filament diameters of 7–18 μm. However, the quadruple extrusion composites of Cline *et al.*[12] exhibited a decrease in J_c as the filament size was taken below 160 nm. This suggests that alternative scaling relations may be required to describe flux pinning in these materials. The present study defines Nb filament properties as a function of annealing history by examining the transport and critical temperature behavior of coarse- and fine-filament Cu-Nb composites given heat treatments at 200–900 °C.

II. EXPERIMENT

The continuous-filament composites of this study were fabricated by the Levi process as applied to Cu-Nb composites by Cline *et al.*[13] In this method OFHC Cu tubes are first swaged and drawn onto Nb rods. The resulting monofilament composite is then hex-drawn and cut into segments so that a billet can be assembled by stacking numerous hexes inside a Cu pipe. After the billet is evacuated and welded shut, extrusion and drawing operations are employed to reduce the composite to final wire size. Finer filament sizes can be achieved if additional bundling, extrusion, and reduction cycles are performed. Two composite designs were used in this investigation. The "2.0*K*" composite is a single extrusion design possessing 1956 filaments of 3.1-μm nominal diameter at a 0.0235-cm-diam wire size. The "1.8*M*" compos-

 0021-8979/90/020930-05$03.00

ite is a double extrusion design utilizing 709 colonies of 2479 filaments each to give 1.76×10^6 filaments of 0.11-μ nominal diameter at a 0.0267-cm wire diameter.

The dependence of critical current density on applied magnetic field was measured to ascertain the effects of both fine-filament structure and heat treatment on the superconducting properties of Cu-Nb composites. The measurements were performed at 4.2 K with a four-point probe arrangement. The usual 1-μV/cm transition criterion was used for samples placed in a magnetic field provided by a NbTi superconducting magnet. Most wires were tested at a nominal diameter of 0.026 cm in a transverse field through a current density range of 10^2–10^5 A/cm^2. In all cases the field was set before sweeping the current to obtain a transition.

The critical temperatures of 0.026-cm-diam composites were determined resistively. The specimens were attached to a jig containing a germanium cryothermometer by four solder contacts. The jig was then inserted into a Cu can wound noninductively with resistance wire. Placement of the can and jig assembly in a 25-mm quartz tube allowed evacuation by a mechanical pump prior to the introduction of a small quantity of He transfer gas. After immersion and equilibration of the tube in liquid He, currents were applied to the sample and thermometer. Power was then applied to the heater can to gradually drive the sample through its transition. An overall sample current density of 30 A/cm^2 was chosen to provide a better comparison with the critical current measurements.

III. RESULTS AND DISCUSSION

The superconducting properties of 0.026-cm-diam 2.0K and 1.8M Cu-Nb wires were determined in the as-drawn condition as well as after 2-h heat treatments performed in a vacuum of better than 2×10^{-6} Torr at temperatures ranging from 200 to 900 °C. The overall critical current densities as a function of applied field, J_c vs H, for the 1.8M composite are shown in Fig. 1. As the annealing temperature rises toward 700 °C, the critical current capacity degrades monotonically. The curves for samples heat treated at 701 and 798 °C are essentially the same, whereas a distinctly different character is exhibited by the sample heat treated at the highest temperature.

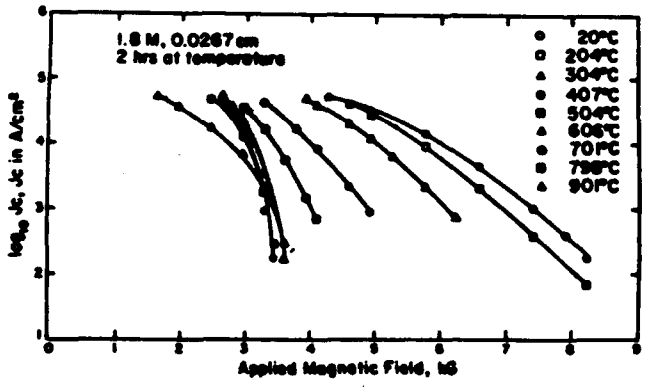

FIG. 1. Logarithm of the critical current density (overall J_c in A/cm^2) as a function of applied magnetic field for fine-filament 1.8M Cu-Nb composites subjected to 2-h heat treatments at various temperatures.

The determination of the scaling laws appropriate to the 1.8M data would allow the definition of the upper critical H_{c_2} effective over the critical current regime investigated. The shape of the as-drawn 1.8M J_c-vs-H curve implies a rapid reduction of the critical current density as the reduced field $h = H/H_{c_2}$ is increased. As in the case of fine-filament Nb_3Sn data,[14] it was found that such behavior failed to fit the Kramer[15] scaling law

$$F_p = J_c' H = K_s \sqrt{h}\,(1-h)^2.$$

Here F_p is the flux pinning force density, J_c' is the critical current density in the filaments, and K_s is a constant for a given sample and temperature. The associated $(1-h)^2$ extrapolation function for H_{c_2} is

$$\sqrt{J_c'\sqrt{H}} = \left(1-\frac{H}{H_{c_2}}\right)\sqrt{\frac{K_s}{\sqrt{H_{c_2}}}}.$$

The higher-order $(1-h)^4$ scaling law employed successfully for the fine-filament Nb_3Sn data is

$$F_p = J_c' H = K\sqrt{h}\,(1-h)^4.$$

The corresponding higher-order extrapolation function becomes

$$\sqrt[4]{J_c'\sqrt{H}} = \left(1-\frac{H}{H_{c_2}}\right)\sqrt[4]{\frac{K}{\sqrt{H_{c_2}}}}.$$

As can be seen in Fig. 2, the $(1-h)^4$ scaling is much more appropriate than the $(1-h)^2$ relation for the as-drawn 1.8M wire. Note the linearity of the H_{c_2} extrapolation function as it indicates an upper critical field of 9.55 kG. The failure of the more common $(1-h)^2$ relation in describing the critical current behavior of as-drawn Cu-Nb wires is not

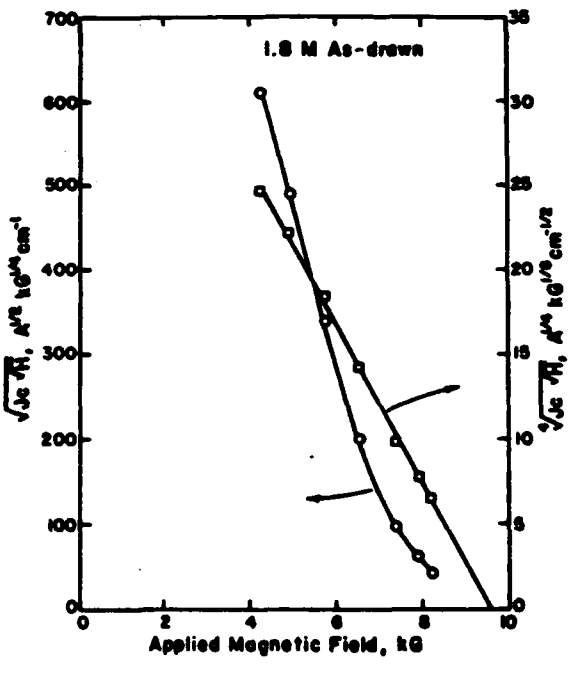

FIG. 2. Determination of H_{c_2} by extrapolation of $\sqrt{J_c\sqrt{H}}$ or $\sqrt[4]{J_c\sqrt{H}}$ to the applied field axis. Linearity implies that $(1-h)^4$ scaling is appropriate for this 1.8M as-drawn sample.

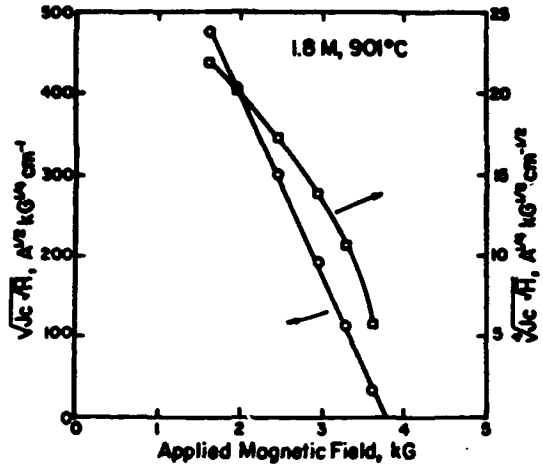

FIG. 3. Determination of H_{c_2} by extrapolation of $\sqrt{J_c\sqrt{H}}$ or $\sqrt[4]{J_c\sqrt{H}}$ to the applied field axis. Linearity implies that $(1-h)^2$ scaling is appropriate for this 1.8M sample heat treated at 901 °C for 2 h.

surprising. As noted in a discussion of Nb_3Sn flux pinning by Evetts and Plummer,[16] there exist serious reservations concerning the applicability of Kramer scaling relations to highly distorted structures. The cold work introduced by drawing to final wire diameter without intermediate anneals will produce a high defect density in the Nb filaments. Only after severe annealing will the internal structure of the Nb become more consistent with the assumptions of the model.

The appropriate scaling relation for the 1.8M composites changes at heat treatment temperatures above 650 °C. The 798 and 901 °C data conform strongly to $(1-h)^2$ scaling. Plots employed for the H_{c_2} determination for the 901 °C sample are shown in Fig. 3. The J_c-vs-H data of this sample conforms closely to the $(1-h)^2$ scaling relation. Similar results hold for the 798 °C sample, whereas the 701 °C sample conforms to either type of scaling only moderately well. A summary of the scaling parameters of the 0.0267-cm 1.8M composite wires is given in Table I. Further reductions in the 1.8M wire diameter resulted in a loss of critical current capacity. As indicated in Table II, the as-drawn wires continued to conform to the higher-order $(1-h)^2$ scaling. However, the degradation in J_c with decreasing wire size

TABLE I. Values of H_{c_2} derived from fitting the 0.0267-cm 1.8M J_c-vs-H data to $(1-h)^2$ or $(1-h)^4$ scaling.

Temperature of 2-h anneal (°C)	n to fit $F_p = K_n\sqrt{h}(1-h)^n$	Correlation coefficient of fit	H_{c_2} (kG)
as-drawn	4	0.9992	9.55
204	4	0.9953	9.01
304	4	0.9993	7.55
407	4	0.9994	6.02
504	4	0.9996	4.84
606	4	0.9985	4.00
701	4	0.9951	3.73
798	2	0.9994	3.53
901	2	0.9996	3.79

TABLE II. Values of H_{c_2} derived from fitting J_c-vs H data of as-drawn 1.8M wires of various diameters to $(1-h)^4$ scaling.

Wire diameter (cm)	n to fit $F_p = K_n\sqrt{h}(1-h)^n$	Correlation coefficient of fit	H_{c_2} (kG)
0.0267	4	0.9974	9.67
0.0208	4	0.9988	9.01
0.0170	4	0.9980	8.20
0.0135	4	0.9949	6.67

was reflected not only in a reduction of H_{c_2}, but also in declining values of the slope of the extrapolation plots.

The overall critical current as a function of applied field results for the coarse-filament 2.0K composite are only qualitatively similar to those described above. The J_c-vs-H characteristics of 0.0254-cm-diam 2.0K wires given 2-h heat treatments up to 900 °C are shown in Fig. 4. At any given heat treatment condition, the critical current capacity of the 2.0K wires is inferior to that exhibited by their 1.8M counterparts. The scaling behavior of the coarse-filament 2.0K composites is initially quite different than that shown by the fine-filament wires. The critical current behavior of 2.0K wires in the as-drawn condition and those annealed at temperatures below 450 °C is such that the plot of $\log_{10} J_c$ vs H is linear over the current density range investigated. Intermediate heat treatment temperatures result in J_c-vs-H behavior that can be represented by the $(1-h)^4$ scaling discussed above. As before, the highest heat treatment temperatures yield curves that are consistent with $(1-h)^2$ scaling. This allowed the effective upper field to be determined readily for wires given heat treatments above 450 °C. For the wires given less severe heat treatments, the upper critical field was estimated as the applied field that would allow an overall critical current density of 10 A/cm^2. This is consistent with the H_{c_2} values obtained from application of the scaling laws to the other wires in the sense that extrapolation of their curves gives H_{c_2} as the applied field at this current density. The scaling characteristics of the 2.0K wires are noted in Table III. The data indicate that H_{c_2} falls sharply as the heat

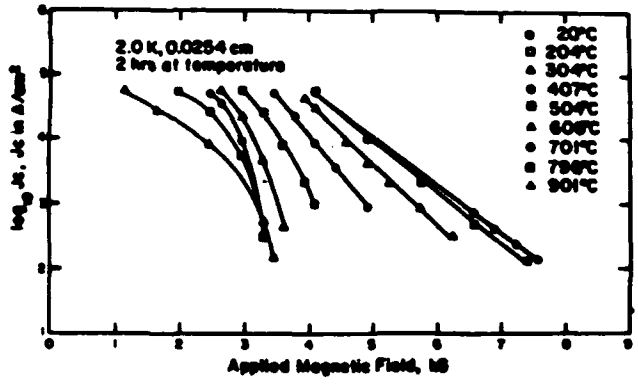

FIG. 4. Logarithm of the critical current density (overall J_c in A/cm^2) as a function of applied magnetic field for coarse-filament 2.0K Cu-Nb composites subjected to 2-h heat treatments at various temperatures.

TABLE III. Values of H_{c_2} derived from fitting the 0.254-cm 2.0K J_c-vs-H data to $(1-h)^2$ or $(1-h)^4$ scaling.

Temperature of 2-h anneal (°C)	n to fit $F_p = K_n\sqrt{h}(1-h)^n$	Correlation coefficient of fit	H_{c_2} (kG)
as-drawn	a	a	9.1
204	a	a	8.7
304	a	a	7.8
407	a	a	6.6
504	4	0.9995	4.79
606	4	0.9982	4.07
701	2	0.9974	3.37
798	2	0.9961	3.45
901	2	0.9992	3.61

[a]The $\log_{10} J_c$-vs-H plot is linear for these samples.

treatment temperature is raised toward 650 °C. As was the case with the 1.8M composite, heat treatment of the 2.0K wires above 650 °C resulted in a limiting value of 3.6 kG for the upper critical field.

The critical temperature T_c of a superconductor is often taken as an indicator of the quality of the material. As a comparison, a Nb single crystal tested at a current density of 3.0 A/cm^2 was found to have a relatively sharp superconducting transition starting at 9.15 K and ending at 9.12 K. The 30-A/cm^2 T_c results for the 1.8M and 2.0K composite wires appear in Fig. 5. Under all heat treatment conditions examined, the transitions for the 2.0K wires are relatively sharp (<0.09 K wide) with the transitions occurring in the vicinity of 9 K. Samples of the 2.0K composite given 2-h heat treatments at temperatures below 400 °C have slightly broadened transitions. Also notable is a significant depression and broadening in the superconducting transitions of samples heat treated above 705 °C. The characteristics of the critical temperature transitions of the 1.8M wires are remarkably different. Under all but the most severe heat treatment conditions, the transitions are quite broad and appreciably depressed. The effect of heat treatment at temperatures below 600 °C is to depress the transition temperature while maintaining the breadth of the transition. Heat treatments above 600 °C tend to increase T_c and sharpen the transition.

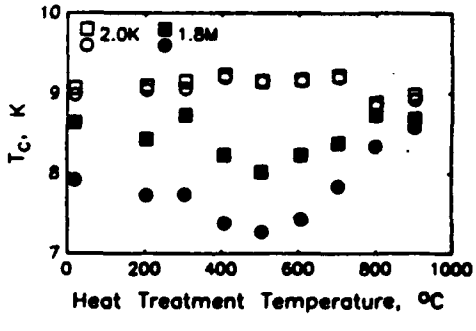

FIG. 5. Critical temperature as a function of 2-h heat treatment temperature for 0.0257-cm 2.0K and 0.0267-cm 1.8M Cu-Nb composite wires. Squares and circles denote the onsets and completions of the transition to the superconducting state, respectively.

IV. CONCLUSIONS

The critical current capacity of cold-drawn Cu-Nb multifilamentary composites is significantly reduced by heat treatment at temperatures as low as 200 °C. Application of the appropriate scaling laws to the coarse-filament 2.0K and fine-filament 1.8M data indicates that the reduction is largely the result of a depression of the effective upper critical field. Shown in Fig. 6 are the effective H_{c_2}'s governing the critical current behavior of the two composites in the range of 100–10^5 A/cm^2. As the heat treatment temperature was raised from 200 to 600 °C H_{c_2} was reduced by more than 1 kG for each 100 °C. Heat treatment at temperatures above 650 °C allowed the upper critical field to reach a limiting value of about 3.4–3.5 kG with some recovery of H_{c_2} after annealing at 900 °C. In addition, the critical current behavior of the 1.8M wires subjected to heat treatments above 750 °C conformed to the more usual $(1-h)^2$ scaling.

The observed changes in H_{c_2} upon annealing would seem to result from a combination of stress relief, recovery processes, and filament coalescence. Stress effects can explain much of the critical current behavior in wires given low-temperature heat treatments. The higher tensile strength and lower volume fraction of the Nb filaments as compared to the Cu matrix allows high residual tensile strains to be introduced in the filaments during cold drawing to final wire size. Differential thermal expansion experiments have shown that the Nb filaments in the present 0.026-cm-diam composites have residual tensile strains of 0.4%–0.75% at room temperature.[3] In the as-drawn wires the tensile stress in the Nb filaments is balanced by compressive stress in the matrix Cu. However, since there is much more Cu than Nb in these composites, the residual compressive stresses in the Cu matrix are of much smaller magnitude than the tensile stresses in the Nb filaments. The higher residual strain levels are associated with the fine-filament 1.8M composite because the greater cold work and smaller interfilament spacings in the fine-filament materials produce a stronger Cu matrix. The effect of heat treatment is to relieve the residual strains by the relatively low temperature annealing of the Cu matrix. Resistivity studies of these composites have shown that 0.026-cm-diam 2.0K wires are fully annealed by heat treatments at less than 500 °C. Fine-filament 1.8M wires of similar diameter experience significant decreases in resistivity beyond 600 °C.[3]

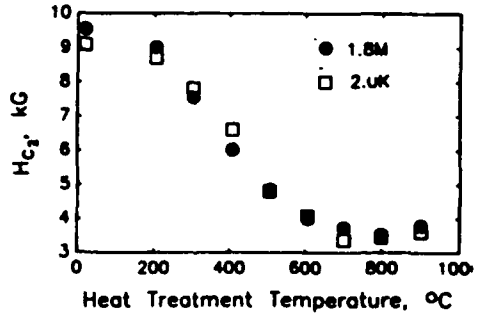

FIG. 6. The effective upper critical field of 0.026-cm 2.0K and 1.8M wires as a function of heat treatment temperature.

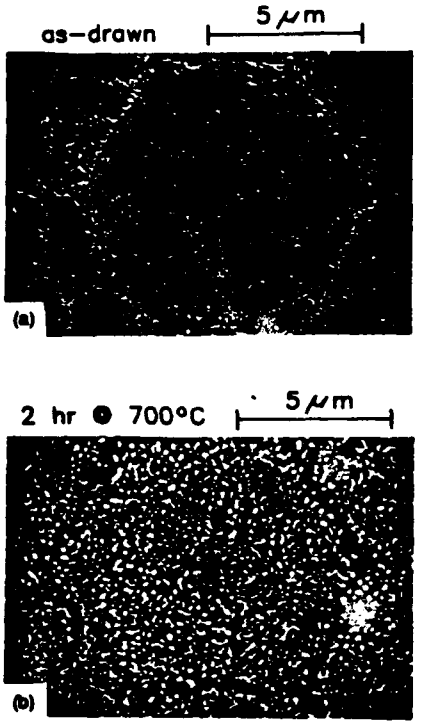

FIG. 7. Cross sections of representative colonies of the 1.8M double extrusion composite are shown (a) in the as-drawn condition and (b) after a 2-h heat treatment at 700 °C. Heat treatment has caused the 2479 Nb filaments of the as-drawn colony to coalesce into a spongelike structure. The matrix Cu has been etched away to reveal the Nb morphology.

The stress state of the Nb filaments is particularly important to the critical current behavior of Cu-Nb composites. The application of tensile strains to as-drawn or heat-treated Cu-Nb composites can drastically enhance the critical current capacity at 4.2 K according to

$$\log_{10} J_c = m\epsilon + b,$$

where ϵ is the applied strain, and m and b are constants for a given sample, applied magnetic field, and temperature conditions.[17] An applied strain of 1% often increases the critical current capacity by more than an order of magnitude. This suggests that the effect of the low-temperature heat treatments of this investigation is to relieve the residual tensile strains in the filaments of the as-drawn wires by permitting relaxation and annealing of the matrix Cu. The lower strain in the Nb filaments results in reduced critical current capacity without internal structural changes in the filaments. This apparent reduction in the upper critical field with reduced filament tension is consistent with the observations of Hill and Rose[18] and Klein.[14]

The present experimental results indicate that heat treatments performed above 400 °C alter the internal structure of the Nb filaments. The Cu matrix of the coarse-filament 2.0K composite will be fully annealed by heat treatments at 450 °C. However, the H_{c_2} values shown in Fig. 6 are still decreasing between 500 and 800 °C. In addition, the 2.0K critical temperature transitions described by Fig. 5 are sharpest between 500 and 700 °C. Similarly, the sharpness and midpoint temperature of the 1.8M superconducting transitions increase with increasing annealing temperature above 500 °C. Microscopic examination of the fine-filament 1.8M composite reveals that high-temperature heat treatments cause the closely spaced filaments to coalesce as shown in Fig. 7. Coalescence of the 1.8M fine-filament colonies would result in large porous "filaments" similar in size to the filaments of the 2.0K composite. This is indicated by the agreement of the 1.8M and 2.0K J_c vs H, H_{c_2}, and T_c behavior in wires heat treated above 550 °C. The action of rapid Nb recovery processes is further supported by electron microscopy of *in situ* Cu-Nb composites. Verhoeven *et al.* have observed the onset of Nb filament coarsening at temperatures as low as 320 °C in fine-filament *in situ* composites.[1] The functional dependence of the critical current on the applied field is determined by the defect structure responsible for flux pinning. Although $(1-h)^2$ scaling is appropriate for wires possessing well-annealed Nb filaments, other relations such as the $(1-h)^4$ scaling noted in this investigation are necessary to describe flux pinning behavior in heavily deformed Nb.

ACKNOWLEDGMENTS

This research was supported by the United States Department of Energy through the Massachusetts Institute of Technology Plasma Fusion Center and by the Defense Nuclear Agency under RDT&E RMSS Code B7661 D SF SB 00034 RAEV 3232 A, DNA Contract No. DNA001-87-C-0150. The authors also gratefully acknowledge the assistance of Irvin Puffer, Dr. S. F. Cogan, and L.R. Granick.

[1] J. D. Verhoeven, H. L. Downing, L. S. Chumbley, and E. D. Gibson, J. Appl. Phys. 65, 1293 (1989).
[2] K. R. Karasek and J. Bevk, J. Appl. Phys. 52, 1370 (1981).
[3] J. D. Klein and R. M. Rose, J. Appl. Phys. 61, 2212 (1987).
[4] J. W. Ekin, Adv. Cryog. Eng. 24, 306 (1978).
[5] C. C. Koch and D. S. Easton, Cryogenics 17, 391 (1977).
[6] W. Schlump, H. Freyhart, and E. Nembach, Acta Metall. 20, 257 (1972).
[7] R. Bormann, J. Appl. Phys. 54, 1479 (1983).
[8] J. D. Verhoeven, E. D. Gibson, F. C. Laabs, J. E. Ostenson, and D. K. Finnemore, IEEE Trans. Magn. MAG-19, 563 (1983).
[9] A. T. Santhanam, J. Mater. Sci. 11, 1099 (1976).
[10] E. J. Kramer, J. Appl. Phys. 44, 1360 (1973).
[11] M. P. Mathur, M. Askin, and D. W. Deis, J. Appl. Phys. 45, 3627 (1974).
[12] H. E. Cline, B. P. Strauss, R. M. Rose, and J. Wulff, J. Appl. Phys. 37, 5 (1966).
[13] H. E. Cline, B. Strauss, R. M. Rose, and J. Wulff, Trans. Q. 59, 132 (1966).
[14] J. D. Klein, Sc.D. thesis, Department of Materials Science and Engineering, M.I.T., Cambridge, MA (1984).
[15] E. J. Kramer, J. Electron. Mater. 4, 839 (1975).
[16] J. E. Evetts and C. J. G. Plummer, in *Proceedings of International Symposium on Flux Pinning and Electromagnetic Properties in Superconductors*, edited by T. Matsushita, K. Yamafuji, and F. Irie (Matsukuma, Fukuoka, 1986), p. 146.
[17] J. D. Klein and R. M. Rose, J. Appl. Phys. 61, 2979 (1987).
[18] D. C. Hill and R. M. Rose, Metall. Trans. 2, 1433 (1971).

DISTRIBUTION LIST

DNA-TR-90-170

DEPARTMENT OF THE ARMY

ABERDEEN PROVING GROUND
ATTN: AMSLC-VL-DE R REITZ

ELECTRONICS TECH & DEVICES LAB
ATTN: PULSE POWER CTR S LEVY
ATTN: SLCET-D C THORNTON

HARRY DIAMOND LABORATORIES
ATTN: F AGEE
ATTN: G HUTTLIN
ATTN: M BUSHELL
ATTN: SLCH-D S GRAYBILL
ATTN: SLCHD-NW-R K G KERRIS

DEPARTMENT OF THE NAVY

NAVAL POSTGRADUATE SCHOOL
ATTN: CODE 61SW F SCHWIRZKE

NAVAL RESEARCH LABORATORY
ATTN: CODE 4000 DR W ELLIS
ATTN: CODE 4700 S OSSAKOW
ATTN: CODE 4720 J DAVIS
ATTN: CODE 4720 J THORNHILL
ATTN: CODE 4770 G COOPERSTEIN
ATTN: CODE 4770 R COMMISSO
ATTN: CODE 4771 P OTTINGER
ATTN: CODE 4774 J R BOLLER
ATTN: CODE 4775 R FORD
ATTN: D MOSHER
ATTN: J NERI
ATTN: R TERRY CODE 4721

NAVAL STUDIES BOARD
ATTN: CAPT J WILSON USN RET

NAVAL SURFACE WARFARE CENTER
ATTN: V L KENYON H23

NAVAL SURFACE WARFARE CENTER
ATTN: CODE F-12 R DEWITT
ATTN: CODE F-12 R GRIPSHOVER

DEPARTMENT OF THE AIR FORCE

AIR FORCE OFFICE OF SCIENTIFIC RSCH
ATTN: MAJ B SMITH

AIR WEATHER SERVICE, MAC
ATTN: AWS TECH LIBRARY FL4414

PHILLIPS LABORATORY
ATTN: AWP J DEGNAN
ATTN: WL/AWP WILLIAM L BAKER

WRIGHT RESEARCH & DEVELOPMENT CENTER
ATTN: POOC R THIBODEAUX
ATTN: POOX-3 OBERLY

DEPARTMENT OF ENERGY

LOS ALAMOS NATIONAL LABORATORY
ATTN: J BROWNELL
ATTN: I LINDEMUTH
ATTN: CHARLES FENSTERMACHER
ATTN: R REINOVSKY

SANDIA NATIONAL LABORATORIES
ATTN: DIV 1253 D MCDANIEL
ATTN: DIV 2566 J HARRIS
ATTN: J J RAMIREZDEPT 1230
ATTN: KENNETH R PRESTWICH DEPT 1240
ATTN: M BUTTRAM DIV 1248
ATTN: ORG 9340 W BEEZHOLD

OTHER GOVERNMENT

CENTRAL INTELLIGENCE AGENCY
ATTN: OSWR J PINA

NASA
ATTN: J LEE

NATIONAL BUREAU OF STANDARDS
ATTN: R HEBNER

DEPARTMENT OF DEFENSE CONTRACTORS

APPLIED PHYSICAL ELECTRONICS LAB
ATTN: DR W NUNNALLY

AVCO CORPORATION
ATTN: M SIRCHIS

BDM INTERNATIONAL INC
ATTN: L O HOEFT

BERKELEY RSCH ASSOCIATES, INC
ATTN: R KARES
ATTN: S BRECHT

BERKELEY RSCH ASSOCIATES, INC
ATTN: J AMBROSIANO
ATTN: J GEARY
ATTN: N PEREIRA

DEFENSE GROUP, INC
ATTN: M K GROVER

EIC LABORATORIES, INC
2 CYS ATTN: A YEN
2 CYS ATTN: J D KLEIN
2 CYS ATTN: L L WU
2 CYS ATTN: S F COGAN

ENERGY COMPRESSION RESEARCH CORP
ATTN: D S WEIN

FORD AEROSPACE CORPORATION
ATTN: M BURNS

FORD MOTOR COMPANY CORPORATION
ATTN: M MOSBROOKER

FORD MOTOR COMPANY CORPORATION
ATTN: C NAKAYAMA
ATTN: H CROFT

GA TECHNOLOGIES, INC
ATTN: J DEGRASSIE
ATTN: K PARTAIN

HUGHES AIRCRAFT CO
ATTN: DR R SCHUMACHER

JAYCOR
ATTN: B SADLER

KAMAN SCIENCES CORP
ATTN: D MOFFETT

LTV AEROSPACE & DEFENSE COMPANY
2 CYS ATTN: LIBRARY EM-08

MAXWELL LABS, INC
ATTN: A KOLB
ATTN: A MILLER
ATTN: D HASKELL 023
ATTN: D HUSOVSKY
ATTN: E CHU
ATTN: G WILKINSON
ATTN: GERSTEN
ATTN: J ENNIS
ATTN: J GILBERT
ATTN: J SEVIGNY
ATTN: J THOMPSON
ATTN: K WARE
ATTN: M MONTGOMERY
ATTN: M RHODES
ATTN: N LOTTER
ATTN: R WHITE
ATTN: W RIX

MISSION RESEARCH CORP
ATTN: B GOPLEN
ATTN: J BRANDENBURG

PENNWALT CORPORATION TECHNOLOGICAL CENTER
ATTN: DR L WEMPE
ATTN: DR P NANNELLI

PHYSICS INTERNATIONAL CO
ATTN: ACP PROGRAM MANAGER
ATTN: C STALLINGS
ATTN: E MOORE JR
ATTN: J GOYER
ATTN: J LEVINE
ATTN: J RIORDAN
ATTN: P SINCERNY

POLYTECHNIC UNIVERSITY
ATTN: R THORSEN

PULSE SCIENCES, INC
ATTN: D JOHNSON
ATTN: I D SMITH
ATTN: J DOUGLAS
ATTN: J LIDESTRI
ATTN: L DEMETER
ATTN: P W SPENCE
ATTN: V BAILEY

R & D ASSOCIATES
ATTN: J BICFORD

S-CUBED
ATTN: A WILSON
ATTN: DR PARKS
ATTN: E KENNEDY
ATTN: E WAISMAN
ATTN: ERIC SALBERTA
ATTN: HYLTON MURPHY
ATTN: I KATZ
ATTN: P STEEN
ATTN: R LAFRENZ
ATTN: RANDALL INGERMANSON

SCIENCE APPLICATIONS INTL CORP
ATTN: D ARION
ATTN: R RICHARDSON

SRI INTERNATIONAL
ATTN: S SCHNEIDER

TETRA CORP
ATTN: W MOOENY

TEXAS TECH UNIVERSITY
ATTN: M HAGLER

TRW SPACE & DEFENSE SECTOR SPACE &
ATTN: HL DEPT/LIBRARY

UNIVERSAL VOLTRONICS CORP
ATTN: W CREWSON

W J SCHAFER ASSOCIATES
ATTN: O COLE III

W J SCHAFER ASSOCIATES, INC
ATTN: E ALCARAZ

WESTINGHOUSE ELECTRIC CORP
ATTN: J S FLETCHER

WESTINGHOUSE STC
ATTN: A BENNETT
ATTN: C HEYNE
ATTN: C IZZO
ATTN: DR A H COOKSON
ATTN: H SAUNDERS
ATTN: L MANDELCORN
ATTN: M MENDELSOHN
ATTN: R E WOOTTON
ATTN: R HARROLD

3M CENTER
ATTN: D REDMOND
ATTN: R ADAMS

DIRECTORY OF OTHER

AUBURN UNIVERSITY
ATTN: M ROSE
ATTN: R ASKEW

UNIVERSITY OF NEW YORK-BUFFALO
ATTN: R DOLLINGER
ATTN: W SARJEANT

UNIVERSITY OF CALIFORNIA-DAVIS
ATTN: J S DEGROOT